VYSOKÉ UČENÍ TECHNICKÉ V BRNĚ
BRNO UNIVERSITY OF TECHNOLOGY

FAKULTA STROJNÍHO INŽENÝRSTVÍ
FACULTY OF MECHANICAL ENGINEERING

ÚSTAV FYZIKÁLNÍHO INŽENÝRSTVÍ
INSTITUTE OF PHYSICAL ENGINEERING

DEPOZICE GA A GAN NANOSTRUKTUR NA VODÍKEM MODIFIKOVANÝ GRAFENOVÝ SUBSTRÁT
DEPOSITION OF GA AND GAN NANOSTRUCTURES ON GRAPHENE SUBSTRATE TREATED BY ATOMIC HYDROGEN

DIPLOMOVÁ PRÁCE
MASTER'S THESIS

AUTOR PRÁCE — **Bc. Stanislav Bárdy**
AUTHOR

VEDOUCÍ PRÁCE — **Ing. Jindřich Mach, Ph.D.**
SUPERVISOR

BRNO 2016

VYSOKÉ UČENÍ TECHNICKÉ V BRNĚ FAKULTA STROJNÍHO INŽENÝRSTVÍ

Zadání diplomové práce

Ústav:	Ústav fyzikálního inženýrství
Student:	**Bc. Stanislav Bárdy**
Studijní program:	Aplikované vědy v inženýrství
Studijní obor:	Fyzikální inženýrství a nanotechnologie
Vedoucí práce:	**Ing. Jindřich Mach, Ph.D.**
Akademický rok:	2015/16

Ředitel ústavu Vám v souladu se zákonem č.111/1998 o vysokých školách a se Studijním a zkušebním řádem VUT v Brně určuje následující téma diplomové práce:

Depozice Ga a GaN nanostruktur na vodíkem modifikovaný grafenový substrát

Stručná charakteristika problematiky úkolu:

Rozhraní Grafen/Ga a Grafen/GaN se jeví jako velmi perspektivní kombinace materiálů nacházející uplatnění zejména v polovodičovém průmyslu. Metoda CVD přípravy grafenových substrátů má pro průmysl největší aplikační potenciál. Polykrystalické a monokrystalické grafenové substráty lze navíc modifikovat atomy vodíku o nízké energii (0,1-1 eV). Takto modifikovaný povrch grafenu je velmi zajímavý z hlediska studia interakce s kovy (Ga) a polovodiči (GaN), zejména s ohledem na růstové a transportní vlastnosti.

Cíle diplomové práce:

1) Provedení rešeršní studie růstu Ga a GaN strukturovaných materiálů na různé substráty (Si, SiO2, grafen,...).
2) Příprava CVD polykrystalických a monokrystalických grafenový substrátů, které budou navíc modifikovány atomy vodíku o nízké energii (0,1-1 eV).
3) Depozice Ga a GaN ultratenkých vrstev za různých fyzikálních podmínek (tok částic, teplota substrátu, energie částic, …).
4) Analýza připravených vrstev metodami XPS, AFM, SEM a Ramanovou spektroskopií.

Seznam literatury:

B. Eren, T. Glatzel, M. Kisiel, W. Fu, R. Pawlak, Appl. Phys. Lett. 102, 071602 (2013).

Losurdo M., Yi C., Suvorova A., Rubanov S., Kim T., Giangregorio M., Jiao W., Bergmair I., Bruno G., Brown A., ACS NANO, Vol. 8, No 3, p.p. 3031-3041 (2014).

Abstrakt
V tejto práci sme sa venovali štúdiu gália na graféne. Depozície Ga boli vykonané použitím Molekulárnej zväzkovej epitaxie. Pozorovali sme Ramanovo zosilnenie a posun píkov spôsobený individuálnymi Ga ostrovčekmi. Simulácia potvrdila náš predpoklad, že zosilnenie je plazmonickej povahy, ktorá je zároveň hlavným mechanizmom Povrchovo-zosilnenej Ramanovej spektroskopie. Ďalším výsledkom je hydrogenácia grafénu pred Ga depozíciou má vplyv na štruktúru vzorky po depozícii a znižuje difúznu dĺžku atómov Ga.

Summary
In this work we studied gallium on graphene. Depositions were done by Molecular beam epitaxy. We observed Raman enhancement and peak shifts by individual Ga islands. Simulation confirmed our assumption, that the enhancement is based on plasmonics effect that is also the main contribution of Surface-enhanced Raman spectroscopy. Another result is hydrogenation of graphene before deposition does have an effect on Ga structure and reduces diffusion length of Ga atoms.

Kľúčové slová
Ramanovo zosilnenie, SERS, gálium, grafén, molekulárna zväzková epitaxia

Keywords
Raman enhancement, SERS, gallium, graphene, Molecular beam epitaxy

BÁRDY, S.*Depozice Ga a GaN nanostruktur na vodíkem modifikovaný grafenový substrát.* Brno: Vysoké učení technické v Brně, Fakulta strojního inženýrství, 2016. 58 s. Vedoucí Ing. Jindřich Mach, Ph.D.

I declare I have elaborated my master's thesis entitled 'Deposition of Ga and GaN nanostructures on graphene substrate treated by atomic hydrogen' independently, under the supervision of the master's thesis supervisor and with the use of technical literature and other sources of information which are all quoted in the thesis and detailed in the list of literature at the end of the thesis.

Bc. Stanislav Bárdy

I would like to thank my supervisor, Ing. Jindřich Mach, Ph.D., for guiding me in the laboratory throughout the studies and being helpful whenever possible. Thanks to prof. RNDr. Jiří Spousta, Ph.D. for the remarks regarding the thesis. I would also like to thank Ing. Zoltán Édes for simulations and Ing. Martin Konečný for an assistance with Raman measurements. Thanks belongs to TESCAN Brno company for giving me valuable time to do RISE measurements. Finally, I would like to thank my parents for the support during my studies.

Part of the work was carried out with the support of Nanofabrication and Nanocharacterisation Core Facility of CEITEC VUT under the project CEITEC – open access LM2011020.

Bc. Stanislav Bárdy

Contents

1 Introduction

Graphene was the first two-dimensional material ever produced and detected in 2004. Since then, it is extensively studied and has potential for a broad range of electronic and optical applications. But graphene must be adjusted first. As a semimetal with the zero overlap of conductive and valence bands, graphene is lacking desired semiconductor properties. Fortunately, there are ways how to open a band gap, for instance with hydrogen adsorption. Controlling the Fermi level can be achieved by metal adsorption. Gallium acts as n-dopant to graphene and has an outstanding property – not only it almost does not react with graphene chemically, but also reconstructs the graphene layer at the interface. On top of that, Ga on graphene enhances the Raman spectrum so it is possible to use it as the Surface-enhanced Raman spectroscopy (SERS) substrate when detecting other substances of little concentration. Origin of the SERS enhancement is of both electromagnetic (plasmonic) and chemical nature.

Here we study Ga grown by Molecular beam epitaxy (MBE) on Chemical-vapour-deposited graphene at various deposition periods and substrate temperatures. We utilise techniques such as Atomic force microscopy, Scanning electron microscopy, X-ray photoelectron spectroscopy, Energy-dipsersive X-ray spectroscopy and Raman spectroscopy to describe sample compositions and effects of Ga on graphene. Atomic hydrogen present on graphene surface and its effect on Ga deposition is briefly studied as well.

A structure of the thesis is as follows: second chapter deals with the thin film depositions by MBE using effusion cell. In the third chapter, we describe the Raman spectroscopy as a characterisation tool for graphene and review the properties of Ga and GaN on graphene. Fourth chapter describes the process of single-crystal graphene preparation on a copper foil and the transfer to SiO_2/Si substrate. Characterisation of produced Ga deposited on graphene samples is presented in the fifth chapter. The sixth chapter discusses Raman enhancement and Raman peak shifts of individual Ga islands on graphene. In the final chapter, the effects of hydrogenation on the Ga deposition are shortly presented.

2 Thin films

Thin film growth is a branch of surface physics dealing with manufacturing of nanomaterials. Thickness of the films can vary from nanometers to micrometers. Thin film growth proces is called a deposition. The deposition technique is used for preparation and study of new materials in the laboratory and also for making semiconductors, light-emitting diodes (LED) and various coatings in the industry.

2.1 Thin film growth by Molecular beam epitaxy

Molecular beam epitaxy (MBE) is a technique for growing thin epitaxial structures composed of semiconductors, metals or insulators [37]. In MBE, thin films crystallise via reactions between thermal-energy molecules or atoms and the substrate which can be held at elevated temperature. The composition of the grown layers depends on the beam flux from effusion cells, substrate type and its temperature. The growth rate can be as small as one monolayer per couple of minutes. This is low enough allowing surface migration of impinging species on the surface. Relatively simple mechanical shutters in front of the beam sources are used to interrupt the beam fluxes, and thus to control the number of deposited layers with high precision. MBE requires ultra-high vacuum (UHV, $p < 10^{-7}\,\mathrm{Pa}$), so the epitaxial growth obeys non-equilibrium thermodynamics and is governed by the kinetics of the surface processes taking place when the impinging particles react with the topmost layers of the substrate [20].

Techniques of thin film depositions can be divided into two categories depending on the way of precursor species transportation to the substrate:

- Physical deposition techniques – the compounds to be grown are vaporised from polycrystalline or amorphous sources at high temperature, and then subsequently transported to the substrate without any chemical change.
- Chemical deposition techniques – volatile species containing the elements of the film to be grown are produced and transported as the stream of vapour towards the reaction zone lying in the vicinity of the substrate. The gaseous species then undergo chemical reactions or dissociate thermally, to form the reactants which participate in the growth of the film.

As MBE requires UHV there are two vacuum related parameters favourably to define. The mean free path L of the particle in the vacuum is the average distance traversed by the particle between two successive collisions:

$$L = \frac{1}{\sqrt{2}\pi n d^2}, \tag{2.1}$$

where d is the particle's diameter, and n is the concentration of particles in the vacuum chamber:

$$n = \frac{p}{k_\mathrm{B} T}, \tag{2.2}$$

where p is pressure, k_B is the Boltzmann constant and T is temperature. We assume kinetic theory of an ideal gas for mean free path definition (particles are identical point

masses, interaction between particles is neglected, Maxwellian velocity distribution of the particles).

Impinging particle on the substrate may encounter several processes: adsorbtion, desorbtion, migration on the surface and cluster formation as depicted in Fig. 2.1. Surface processes depend on the substrate temperature and interactions between impinging particles and the substrate. There are two types od adsorbtion. Physisorption is interaction where no electron transfer between an adsorbent and the substrate occurs and bonding force is van der Waals type. Much stronger chemisorption is created when electron transfer takes place. Thin film growth can occur in three characteristic modes (Fig. 2.2)

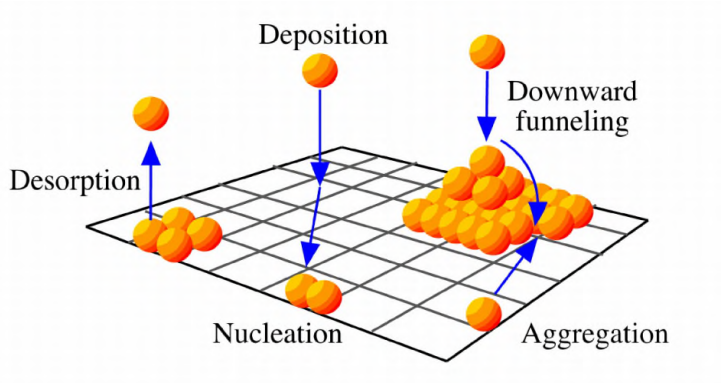

Figure 2.1: Surface processes occuring during MBE. Retrieved from [2].

depending on forces between the growth constituents:

- Volmer-Weber (island formation) - adatom-adatom force is stronger than adatom-surface force resulting in island formation and rough surface
- Frank-van der Merwe (layer-by-layer) - adatom-substrate force overcomes the force between adatoms creating smooth layers
- Stranski-Krastanov (layer plus island) - intermediate mode, transition from layer-by-layer to island formation starts at critical thickness depending on surface energies and lattice parameters

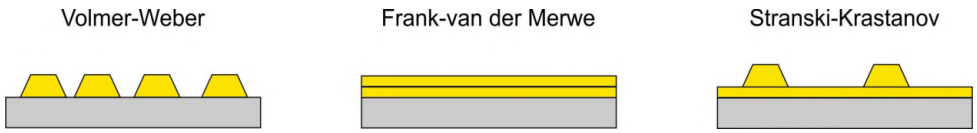

Figure 2.2: Thin film growth modes.

2.2 Effusion cell

As a source in MBE is often used an effusion cell in which deposited material is placed in a temperature controlled crucible. The picture of effusion cell is in Fig. 2.3. Deposited material is evaporated from the crucible toward a substrate. Hertz in 1882 found out that liquid cannot exceed a certain maximum evaporation rate at a given temperature [21].

Evaporation rate as studied by Knudsen led to the formula for maximum evaporation rate also known as Hertz-Knudsen relation

$$\frac{\mathrm{d}N_\mathrm{e}}{A_\mathrm{e}\mathrm{d}t} = a_\mathrm{V}(p_\mathrm{eq} - p)\sqrt{\frac{N_\mathrm{A}}{2\pi M k_\mathrm{B} T}}, \tag{2.3}$$

where dN_e is number of molecules evaporating from the surface area A_e, a_V is the evaporation coefficient, p_eq is the equilibrium pressure, p is hydrostatic presure, M is the molecular weight and T is the temperature of the evaporating substance. Langmuir in 1913 showed that Hertz-Knudsen relation can be also applied to evaporation from free solid surfaces [24].

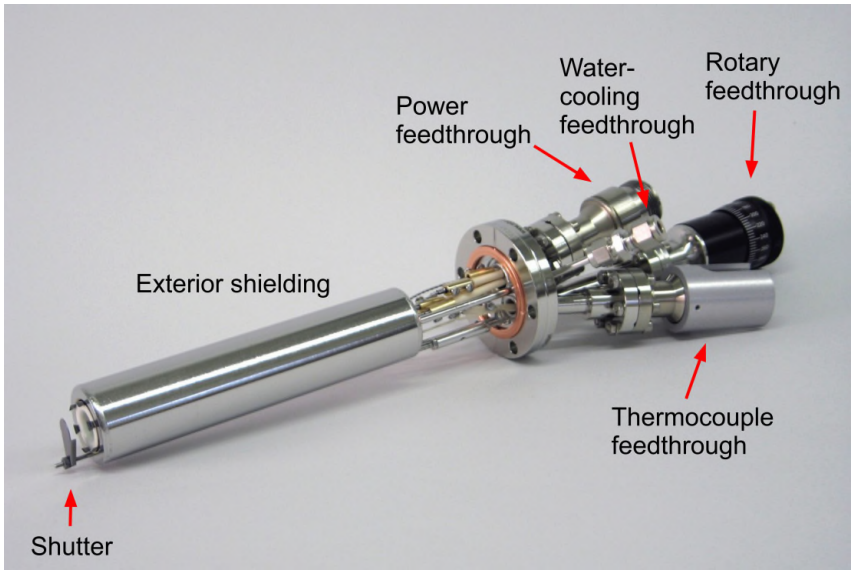

Figure 2.3: Example of an effusion cell. The model from Omicron. Retrieved from [4].

Not all the evaporated atoms reach the sample surface and those that impinge the sample can bounce back. The number of adsorbed atoms to the number of impinging atoms is sticking coefficient, s. If the adsorption process depends on the temperature we are talking about activated adsorption. The sticking coefficient for activated adsorption is

$$s = \sigma f(\theta)\mathrm{e}^{-E_\mathrm{act}/k_\mathrm{B}T}, \tag{2.4}$$

where σ is the condensation coefficient (carrying information about a molecular orientation and energy transfer to the surface), $f(\theta)$ is the coverage function describing the probability of finding an adsorption site and the Boltzmann factor $\mathrm{e}^{-E_\mathrm{act}/k_\mathrm{B}T}$ governs energetics of the adsorption. Often, the sticking coefficient is proportional to the coverage of the substrate with the deposited atoms θ when E_act depends on coverage:

$$s \sim \mathrm{e}^{-\alpha\theta/k_\mathrm{B}T}, \tag{2.5}$$

where α is a constant. Desorption from the surface is described by the desorption rate, r_des – which is a rate of desorbing particles per unit surface

$$r_\mathrm{des} = \sigma^* f^*(\theta)\mathrm{e}^{-E_\mathrm{des}/k_\mathrm{B}T}, \tag{2.6}$$

where σ^* is the desorption coefficient and $f^*(\theta)$ is the coverage dependent function [32].

3 Graphene, Ga and GaN

This chapter deals with the basic properties of graphene and its preparation methods. Next, a brief review of Ga on graphene is provided. At last, current research of GaN on graphene is presented.

3.1 Graphene

Next to diamond, graphite, carbon nanotubes and fullerens, graphene is another carbon allotropy. Describing the band structure of graphite in 1947, P. R. Wallace was the first person who theoretically studied graphene [38]. Almost six decades later in 2004, graphene was isolated, using such a simple equipment as skotch tape and graphite [31]. Graphene opened a door for a range of 2D materials emerged soon after [8]. Graphene is a carbon monolayer formed to a honeycomb lattice as represented in Fig. 3.1. The lattice is defined by vectors:

$$\boldsymbol{a_1} = \frac{a}{2}(3, \sqrt{3}), \tag{3.1}$$

$$\boldsymbol{a_2} = \frac{a}{2}(3, -\sqrt{3}), \tag{3.2}$$

where $a = 1,42\,\text{Å}$ is a distance between two neighbouring carbon atoms in the lattice. For reciprocal lattice (Fig. 3.1 (b)) there are vectors defined as

$$\boldsymbol{b_1} = 2\pi \frac{\boldsymbol{a_2} \times \boldsymbol{n}}{|\ \boldsymbol{a_1} \times \boldsymbol{a_2}\ |} = \frac{2\pi}{3a}(1, \sqrt{3}), \tag{3.3}$$

$$\boldsymbol{b_2} = 2\pi \frac{\boldsymbol{n} \times \boldsymbol{a_1}}{|\ \boldsymbol{a_1} \times \boldsymbol{a_2}\ |} = \frac{2\pi}{3a}(-1, \sqrt{3}), \tag{3.4}$$

where $\boldsymbol{n}$ is a unit vector perpendicular to the graphene plane. Lattice can be also described by two independent triangular lattices which contain A and B atoms. Outstanding me-

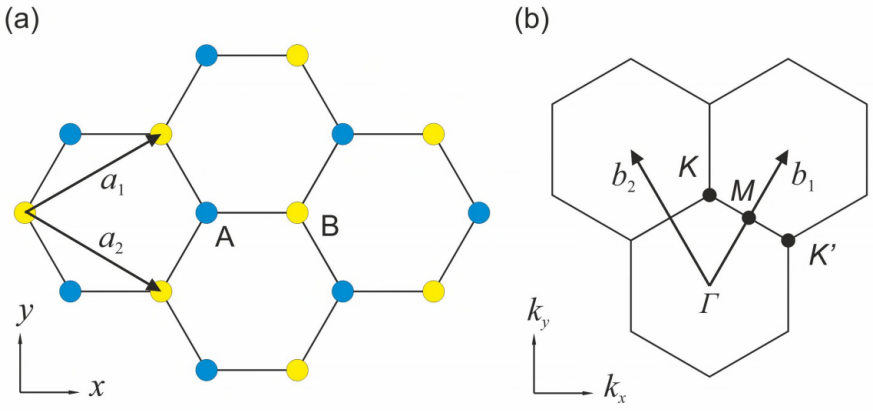

Figure 3.1: (a) Graphene lattice in a real space. A and B atoms form a unit cell. (b) First Brillouin zone of graphene's reciprocal lattice labeled with high symmetry points.

chanical and thermal properties are the results of σ bonds between carbon atoms. Fourth bond is a π bond oriented in the out-of-plane direction. Graphene π bonds are hybridised forming the π- and π^*- bands responsible for remarkable electronic characteristics. These

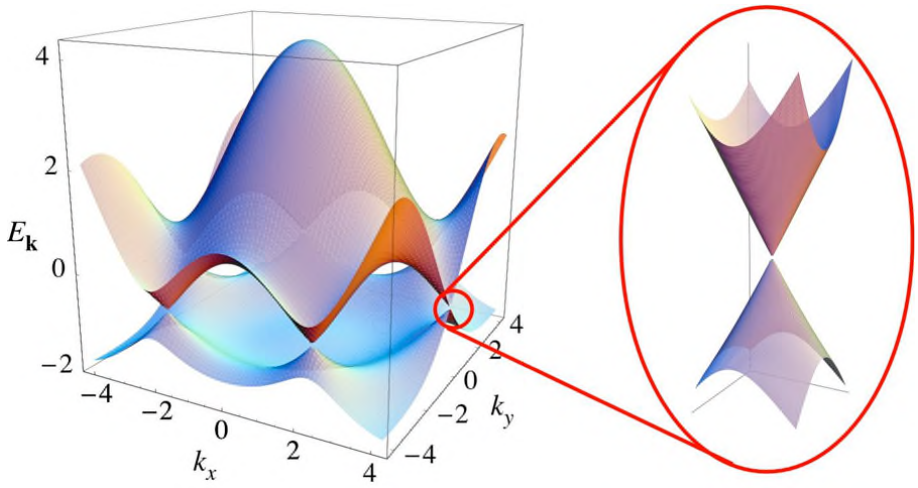

Figure 3.2: Energy-momentum diagram of the uppermost occupied and the lowermost empty bands. The reason of such extensive studies on graphene is the characteristic cone meeting at the Dirac point. Unlike the semiconductor parabolic dispersion, graphene it has linear reminding the photon dispersion relation. Retrieved from [30].

bands are linearly dispersed and meet on the edge of the Brillouin zone at K (K' resp.) point known as the Dirac point in Fig. 3.2. Linear dispersion near the K point is derived from the tight-binding-model and is described by energy dispersion relation for massless fermions:

$$E_{\pm}(k) \approx \pm\hbar v_{\mathrm{F}}|k - K|, \tag{3.5}$$

where v_{F} is Fermi velocity. Graphene is a zero band gap semiconductor and for using it in the electronic circuits the band gap must be opened and controlled. It can be done in several ways. Atomic hydrogen adsorption opens a gap in the electronic density of states [13]. Creating a pattern of holes inducing systematic defects into the graphene lattice is another way how to open a band gap [33]. Substrates such as boron nitride can also influence a band gap [19].

3.1.1 Preparation techniques

Since graphene discovery, there were developed several ways of graphene preparation. Here are the most important of them:

Mechanical exfoliation

A skotch tape is used to peel off layers of graphite from a highly oriented pyrolitic graphite. Then graphite on the skotch tape is peeled off repeatedly to obtain only few graphene layers. Finally, the skotch tape is put on the silicon substrate with thick layer of SiO_2. Although, graphene monolayer absorbs only 2.3% of light, it is possible to see the graphene flake in the optical microscope due to interference caused by a precisely thick layer of SiO_2. The size of graphene flakes may be up to several μm and their quality is excellent, practically without defects. However, production and location of single flakes is time demanding and suitable mainly for scientific research.

Chemical vapour deposition

Chemical vapour deposition (CVD) is production process that forms solids from vapour precursors at elevated temperature. Graphene is grown on Ni or Cu substrates acting as catalysators for the growth reaction. Graphene grown on Cu has larger area and contains more homogenous layer than graphene on Ni substrate [40], therefore Cu as the substrate is more promising in CVD grown graphene. General recipe is annealing of 25 μm Cu foil in hydrogen atmosphere at about 1000 °C. Then a H_2/CH_4 mixture is introduced into the furnace to initiate the graphene growth. After forming the graphene layer, a furnace is cooled down to room temperature. Next, graphene is transferred to a non-conductive substrate like glass or SiO_2 using poly(methyl methacrylate) (PMMA). Advantage of CVD method is production of very large graphene films at relatively low cost. On the other hand, wet transfer from moteal to another substrates leaves graphene with PMMA residue and degrades its quality.

Thermal decomposition of SiC

Another way of preparing graphene is epitaxially when graphene layers are formed on the top of thermally decomposed SiC. Firstly, SiC is annealed in H_2 at around 1000 °C and then the temprature is risen to 1600 °C when Si atoms sublime and C atoms reconstruct to form graphene layers. A rate of Si sublimation is controlled by Ar atmosphere. While the Si face of SiC is covered by a monolayer graphene, on the C face a few dozens of layers are formed [6]. Si dangling bonds below graphene are source of electrons and epitaxial graphene is thus n-doped which shifts the Fermi level upwards. There is no need to transfer epitaxial graphene since it grows directly on insulating substrate and its size is limited only by a wafer size. Cost of SiC wafers is rather high.

Reduction from graphene oxide

Graphite oxide is highly oxidised form of graphite with bigger inter-layer spacing than regular graphite due to oxygen functionalities. Ultrasonication of graphite oxide in a polar organic solvent leads to the separation of graphite oxide layers to mono- and few-layer graphene oxide films. Graphene oxide films then can be reduced to graphene by several methods: exposing to H_2 plasma, heating, treating with hydrazine hydrate and many other reducing agents as reviewed in [9]. Ultrasonication of graphite oxide cause tearing graphene oxide films apart to a few μm^2 and also degrades quality of layers.

Liquid phase exfoliation from graphite

This mehod is similar to the previous one but it uses graphite instead of graphite oxide. Graphite is ultrasonicated in mixture of dimethylformamide and water to form graphene sheets [41]. Unexfoliated graphite is removed by a centrifuge and supernatant is pipetted off. Advantage of this method when compared to the reduction of graphene oxide is the absence of oxygen functionalities. A general disadvantage of the technique is low quality of graphene layers.

3.2 Raman spectroscopy

Raman spectroscopy is an optical technique for observing low frequency vibration modes in a system. It was first studied in 1928 by C. V. Raman and for this work he was awarded with Nobel prize in 1930 [35]. Raman spectroscopy is based on the Raman scattering where small part (10^{-7}) of the monochromomatic light is scattered inelastically by phonons. Raman scattering occurs when energy of the molecule is changed due to transition to virtual energy level. Virtual energy levels are not stationary and the molecule undergo deexcitation soon. When the frequency of emitted photon is lower or higher than the energy of incoming photon we are talking about Stokes shift or anti-Stokes shift (Fig. 3.3). Graphene has two atoms per unit cell, thus we consider six coordinates producing six

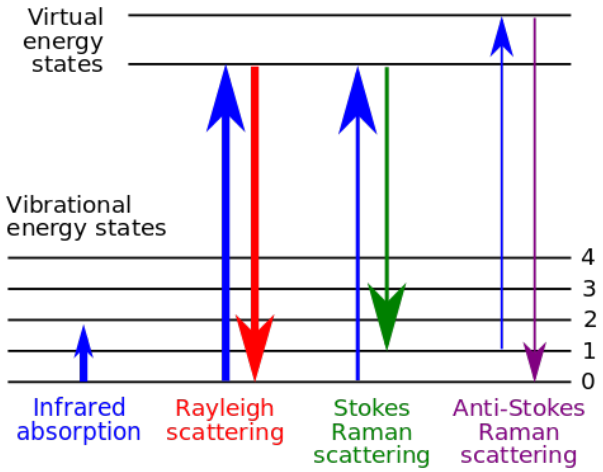

Figure 3.3: States involved in Raman signal. Rayleigh scattering signal is blocked out before reaching the detector. Retrieved from [1].

normal phonon modes. Graphene has three characteristic peaks in its Raman spectrum. G peak ($\sim 1585\,\mathrm{cm}^{-1}$, measured CVD graphene on SiO_2) corresponds to degenerate in-plane mode, E_{2g}, at Γ point in the Brillouin zone [36]. It does not vary with changing number of graphene layers much. D peak ($\sim 1345\,\mathrm{cm}^{-1}$) emerges when defects in graphene are present. It is not present in perfect graphene layer because of crystal symmetries [36]. Its intensity increases with defect density. 2D peak ($\sim 2670\,\mathrm{cm}^{-1}$) is D peak overtone. It is always present in graphene even if there are not defects due to two phonons process with opposite momenta. Phonons are located in the highest optical branch near the K point. Increasing the number of graphene layers broadens the 2D peak [16, 17]. Both D and 2D peaks are dispersive [15] Typical Raman spectra of graphene and graphite (a) together with the spectrum of defected graphene (b) are shown in Fig. 3.4. Defected graphene means

Raman spectrum of monolayer graphene depends on various factors such as gate voltage (doping) [11], temperature [7], functionalisation by adsorbed particles [28] and lattice strain [27]. Dependence on gating (doping) is shown in Fig. 3.5. G peak tends to shift to higher wavenumbers when Fermi level is moved away from the Dirac point. Intensity of the G peak depends on doping very weakly. On the other hand, dependence of the 2D peak on electron-electron interaction results in lowering its intensity when graphene is doped. 2D peak move from higher to lower wavenumbers as graphene's doping changes from p (negative gating) to n (positive gating) [11].

When stress is applied to lattice the phonon frequency in Raman process changes. Tensile strain causes decreasing decreasing of the phonon frequency resulting in red shift of the Raman spectra and compressive strain increases the phonon frequency and blueshifts the Raman spectrum. G peak splits into two peaks when monolayer graphene is undergoing tensile and compressive strain. Red-shifted Raman peaks of graphene under tensile strain are in Fig. 3.6.

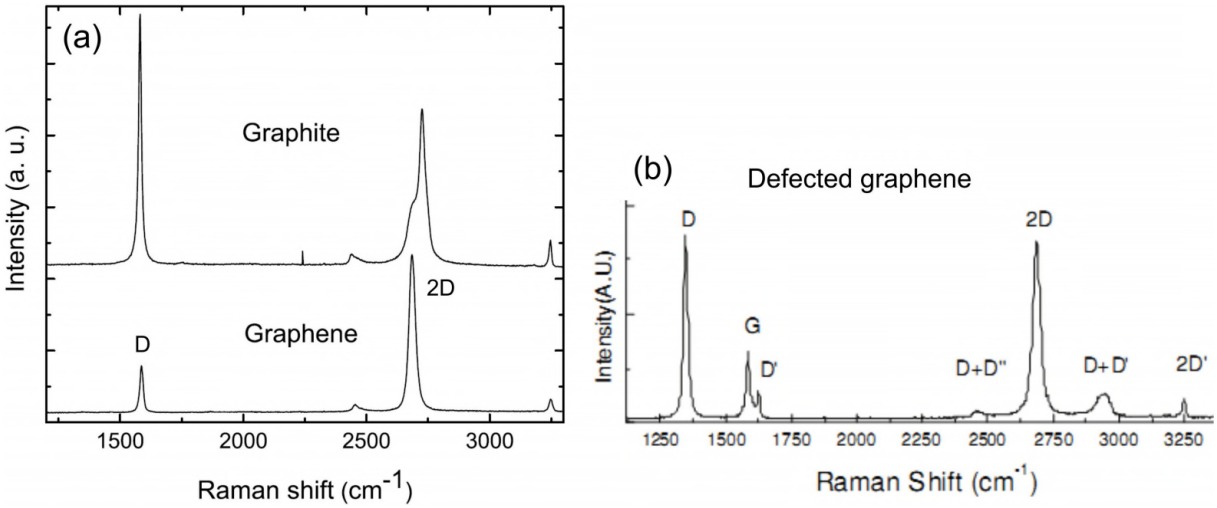

Figure 3.4: Raman spectra of carbon materials. (a) Graphene and graphite spectra [17]. (b) Spectrum of defected graphene with [16]. Typical peaks are labeled.

3.3 Hydrogentated graphene

Chemical modification of graphene is a method how to tune its electronic properties. One way of chemical modification is hydrogen adsorption. Atomic hydrogen sits on graphene lattice and change carbon sp^2 to sp^3 bond. Sources of hydrogen can be plasmatic, chemical or thermal cracking of molecular hydrogen.

Placing an exfoliated graphene sample to hydrogen plasma changes its Raman spectrum causing rise of the D peak and increases resistance. Annealing the sample at 450 °C in Ar for 24 h removes hydrogen as seen in the Raman spectrum and resistance measurements [14]. But the D peak from Raman spectrum is not totally diminished suggesting reactive plasma species cause irreversible defects to graphene as shown in Fig. 3.8. Furthermore, hydrogenation caused lateral compression of graphene membranes by 5%. At Eindhoven University of Technology we studied hydrogenated epitaxial graphene on SiC(0001). Hydrogenation was performed using thermal cracker which turns molecular hydrogen into atomic. Fractal-like structure emerged on graphene upon hydrogenation as can be seen in Fig. 3.7. Hydrogenation of epitaxial graphene creates magnetic fields and the system shows ferromagnetic properties [18]. In academic world there are currently no scientific papers on experimental hydrogenation of CVD graphene by atomic hydrogen.

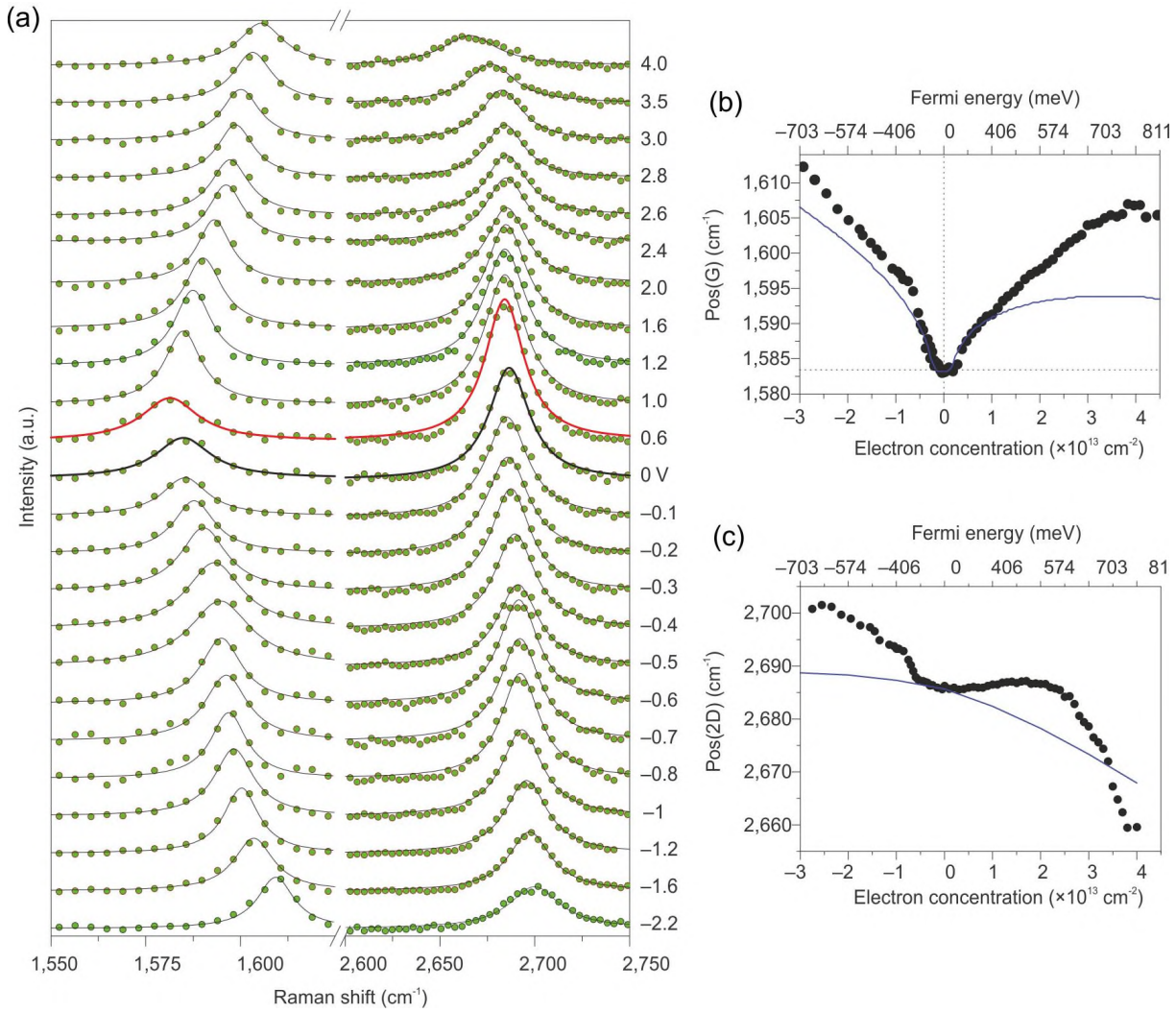

Figure 3.5: (a) Raman spectra of graphene as a function of top gate voltage. Dots are experimental data, curves are lorentzians. (b), (c) are G and 2D peak positions as a function of doping. Blue lines are DFT calculations. Retrieved from [11].

3.4 Gallium on graphene

Gallium is a soft, silvery metal with atomic number $Z = 31$ and with characteristically low melting point $T_{\mathrm{M}} = 29.76\,^{\circ}\mathrm{C}$. In nature, Ga occurs as a trace element in bauxite and sphalerite. Application of Ga is mostly in electronics as a GaAs in electronic circuits. Next to it, GaN and InGaN are used as light-emitting diodes.

Effects of C substitution by Ga atoms and Ga adsorption on graphene are various. Introducing dopant into graphene lattice breaks perfect symmetry which results in the band gap opening. Ga and Ge incorporation into graphene lattice was studied using density functional theory [12]. In this work, the parameter 'formation energy'(FE) represents incorporation of dopant into graphene. Lower FE is related with better incorporation of the dopant into the graphene lattice. Substitutional doping of graphene with Ga exhibits large formation energy which means small disturbance of the lattice. Ga doping displays a reactivity that is larger than that corresponding to a double vacancy. At some concentrations, Ga doping induces a half metallic behavior. FE for Ga doped graphene is 2.81 eV and 0.23 eV for Ge doped graphene (one dopant atom per 4×4 graphene unit

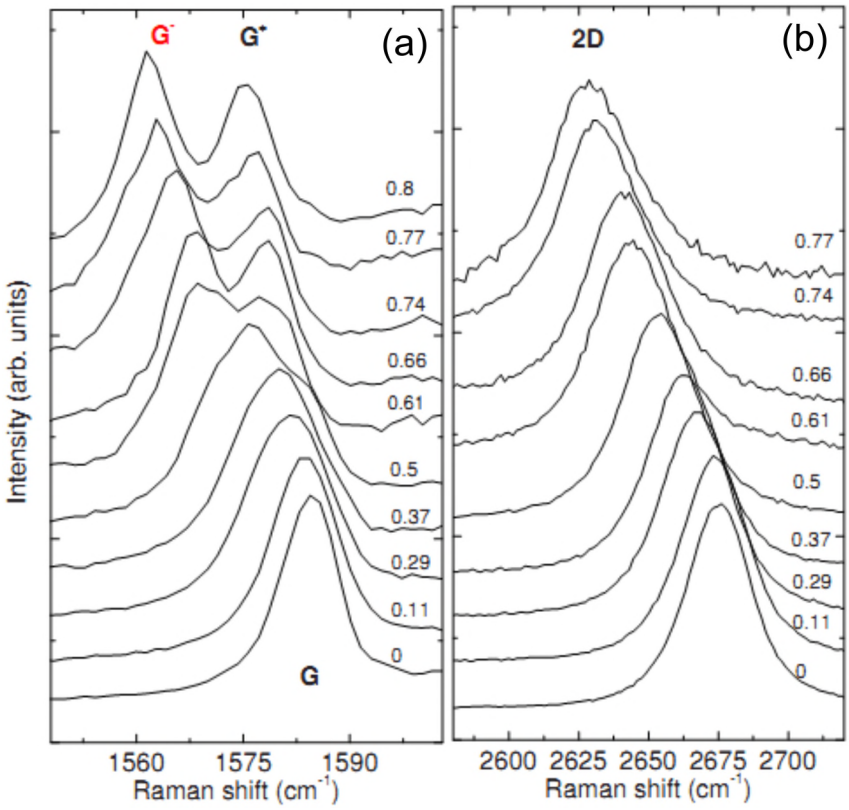

Figure 3.6: (a) G and (b) 2D Raman peak evolution as a function of applied tensile strain. G peak splits into G^- and G^+. The strain value in % is on the right side of each graph. Retrieved from [27].

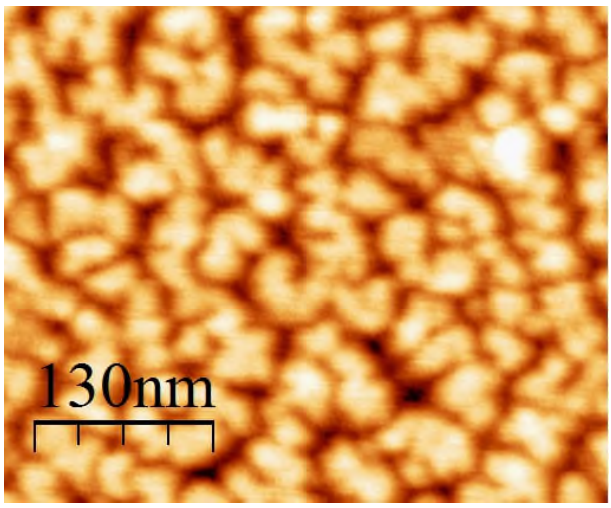

Figure 3.7: AFM topography image of hydrogenated epitaxial graphene. Z scale is 2 nm. Measured during the internship at Eindhoven University of Technology.

cell). Ge manifests small FE as consequence of similar electronic structure of Ge and C. The dopant protrudes out of the graphene plane, because it is too big to fit into the sp^2-hybridized graphene lattice. Ga and Ge are located 0.18 nm and 0.17 nm respectively above the lattice (lattice constant of graphene is 0.142 nm). Band gap created by Ga doping is 0.2 eV and 0.4 eV by Ge atom substitution. Ga has a significant effect on chemical reactivity (hydrogen atom addition) of graphene due to the charge redistribution and

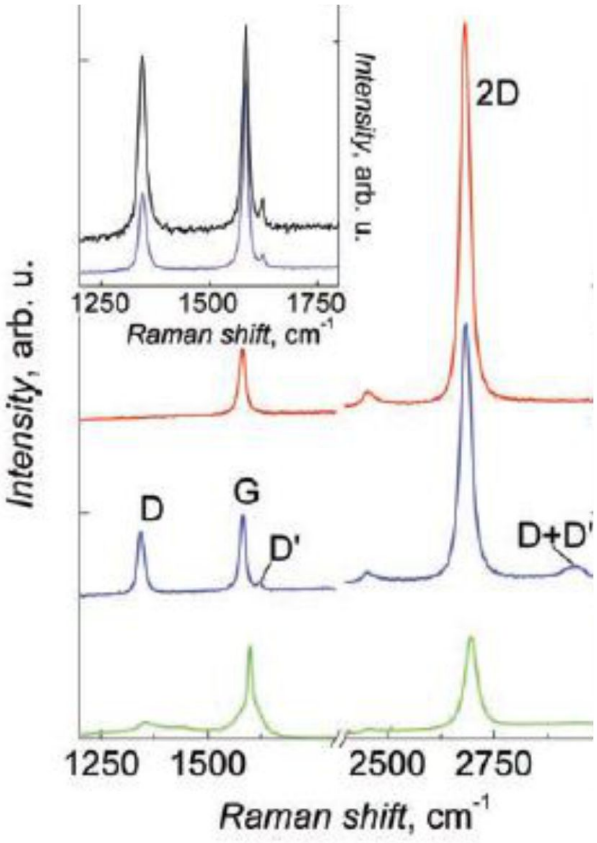

Figure 3.8: Raman spectra of pristine (red), hydrogenated (blue) and annealed (green) epitaxial graphene on SiO_2. Annealing was at 450 ° in Ar atmosphere for 24 h. D, D' and D+D' peaks are related to defects caused by hydrogenation. Inset: comparision of single- and double-side exposure to hydrogen. Retrieved from [14].

leaving of the unpaired electron by Ga atom introduction to the lattice. Binding energy of H to the Ga doped graphene is 4.1 eV higher than to the pristine graphene.

In [39] Yi's group studied localised surface plasmon resonance (LSPR) of Ga nanoparticles on epitaxial graphene. Bi- or tri-layer graphene was grown on C face of 4H-SiC. Ga was deposited via MBE at room temperature. Upon deposition of Ga NPs, they did not observe broadening of XPS peaks or any new carbide peaks related to Ga carbides, indicating that Ga does not react with graphene and the adsorption is the result of ionic attractive interaction between p orbitals of Ga and π orbitals of graphene. The only observed variation in the C1s peak was the attenuation of the graphene and SiC contributions and a further shift to lower binding energy (closer to Fermi level) with increasing Ga amount, indicating electron transfer from graphene to Ga. After Ga deposition, enhancement of graphene Raman modes were observed. The D peak had the largest enhancement followed by that of the 2D band, while the in-plane vibrational G band had the smallest enhancement as shown in Fig. 3.9. D and G peaks were blueshifted (increase of energy). They argue that large enhancement observed for the D mode is not likely to be caused by additional graphene defects generated by Ga deposition, since no D peak appeared upon Ga deposition on exfoliated graphene.

Losurdo et al. [25] observed enhanced Raman intensity of Ga on graphene. They used CVD graphene on SiO_2 and 82 Ga monolayers were deposited by MBE at room temperature. XPS spectra (Fig. 3.10) revealed rise of Ga metallic states upon Ga deposition

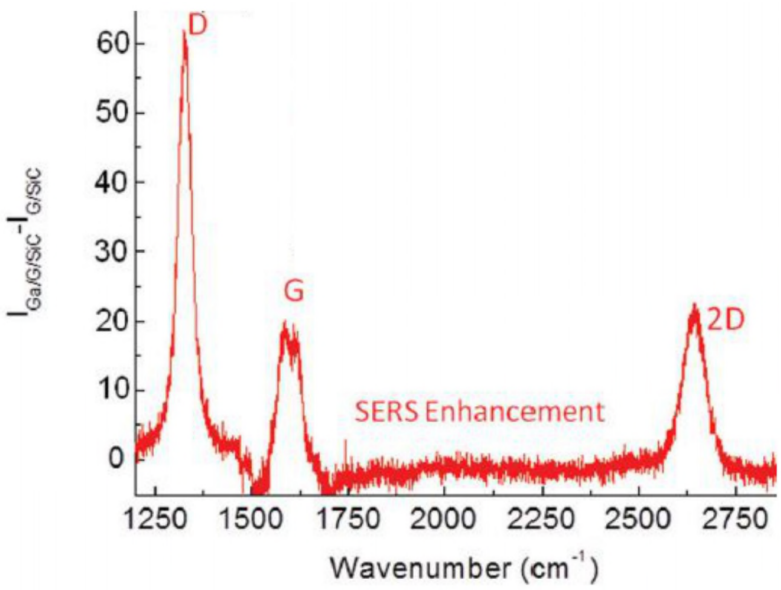

Figure 3.9: Enhanced Raman peaks after Ga deposition on epitaxial graphene grown on C-face SiC. Here, the enhancement is Raman intensity difference of sample with and without Ga. Retrieved from [39].

on graphene/SiO_2/Si. Meanwhile, XPS signal from graphene σ bands did not increase, suggesting these graphene states did not rehybridize with Ga. Delocalised π states of graphene were increased because of electron transfer from Ga to graphene. Radius of Ga spheres increased with deposited volume. Gaussian distribution of Ga spheres broadened with increasing deposition time. Raman spectra revealed D peak formed upon Ga deposition ($I_D/I_G = 0.15$) which was the consequence of small disturbance of graphene lattice. Enhancement in the Raman intensity was assigned to Surface-enhanced Raman scattering (SERS) at Ga/graphene interface. SERS exploits enhancement of the Raman signal when metallic particles are adsorbed on the substrate. Still, the precise mechanism of SERS is a matter of debates. Electromagnetic theory proposes excitation of localised surface plasmons, whereas chemical theory supports charge transfer. Back to the paper, G and 2D peaks increased with increasing both Ga sphere size and coverage as shown in Fig. 3.11. Slightly larger enhancement for 2D peak was attributed to its intensity dependence on electron-electron interactions which could change with Ga adsorption. They claim both electromagnetic and chemical contribution to the SERS but due to electron transfer from Ga to graphene the EM enhancement would be lower by orders of magnitude. Furthermore, with increasing Ga sphere size, both the G and 2D peak positions shift $3 - 5\,\mathrm{cm}^{-1}$ to lower wavenumbers.

3.5 Gallium nitride on graphene

Gallium nitride is a very hard material with wurtzite crystal structure. It is a direct bandgap semiconductor. A width of the bandgap is quite large, 3.4 eV. GaN was used in fabricating of the first efficient blue light-emitting diode (LED) next to already existing red and green LEDs. Akasaki, Amano and Nakamura were awarded with Nobel prize for their work on the blue LED in 2014. The discovery of blue LEDs finally allowed producing high-efficient white light sources used all around us.

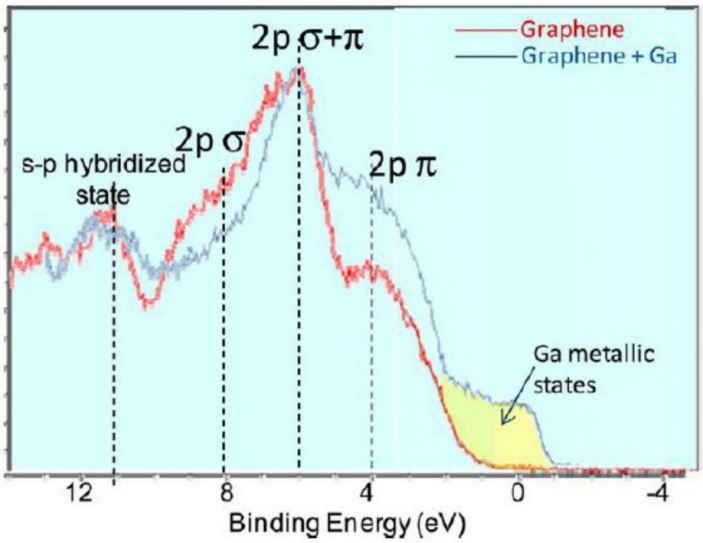

Figure 3.10: XPS spectrum of CVD graphene sample prior and after Ga deposition. Retrieved from [25].

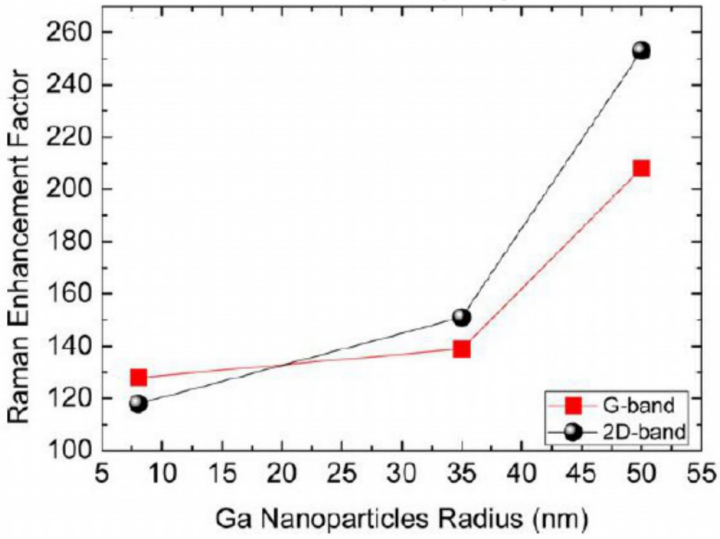

Figure 3.11: Raman enhancement of characteristic graphene peaks with adsorbed Ga. Enhancement is defined as the ratio of the Raman intensity of Ga deposited graphene and pristine CVD graphene. Retrieved from [25].

GaN is mechanically stable material with large heat capacity and thermal conductivity. Next, as GaN has much larger band gap than Si (1.12 eV), it has higher operating temperature and higher breakdown strength and is better option for usage in power supply circuits. Comparision of GaN to GaAs and Si is in Fig. 3.12. Graphene used as the substrate for GaN growth is interesting due to similarity of hexagonal arrangement of the carbon atoms to the c-plane of wurtzite GaN as shown in Fig. 3.13. In addition, group-III metals on graphene have low migration barrier enabling large diffusion lengths and thus creation of large islands coalescensing into films with reduced dislocations. Challenge is to overcome a lack of chemical reactivity between nitrides and graphene.

On the other hand, graphene can be used as the interface medium between the substrate and GaN to partially block propagation of defects from conventional substrates like Si or Al_2O_3. Zhang et al. [40] studied how graphene nanosheets can improve the

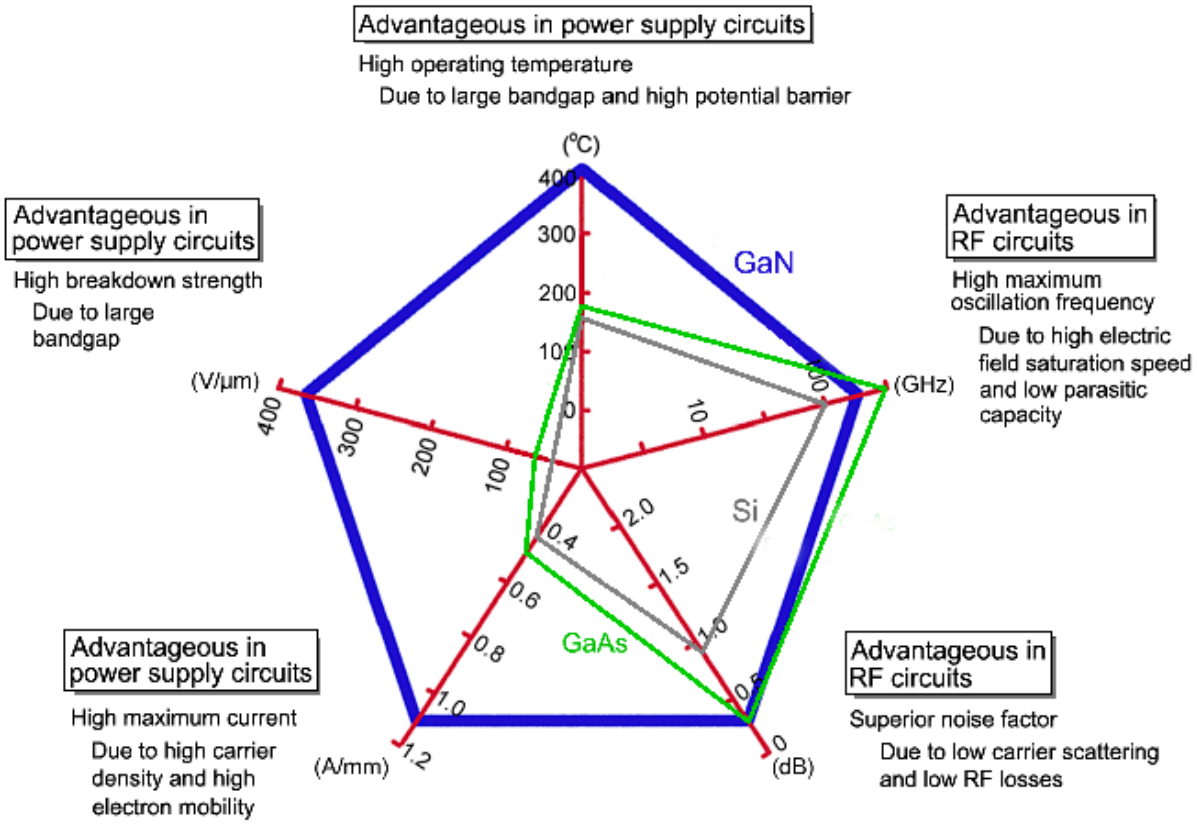

Figure 3.12: Comparision of GaN to GaAs and Si. Retrieved from [3].

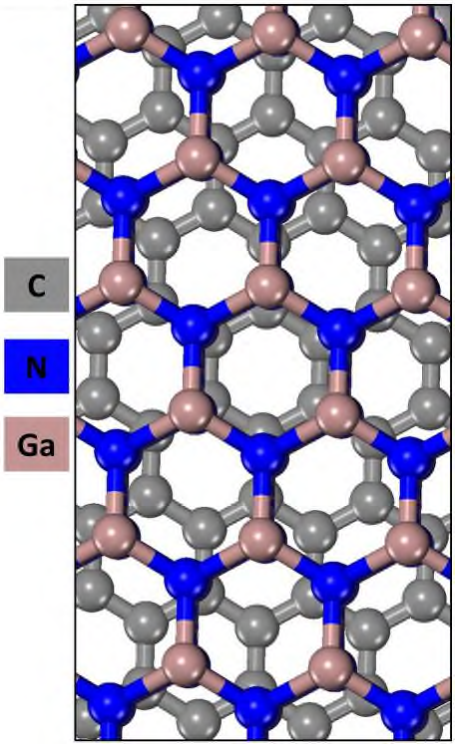

Figure 3.13: Density functional theory simulation of relaxed GaN on graphene. Retrieved from [5].

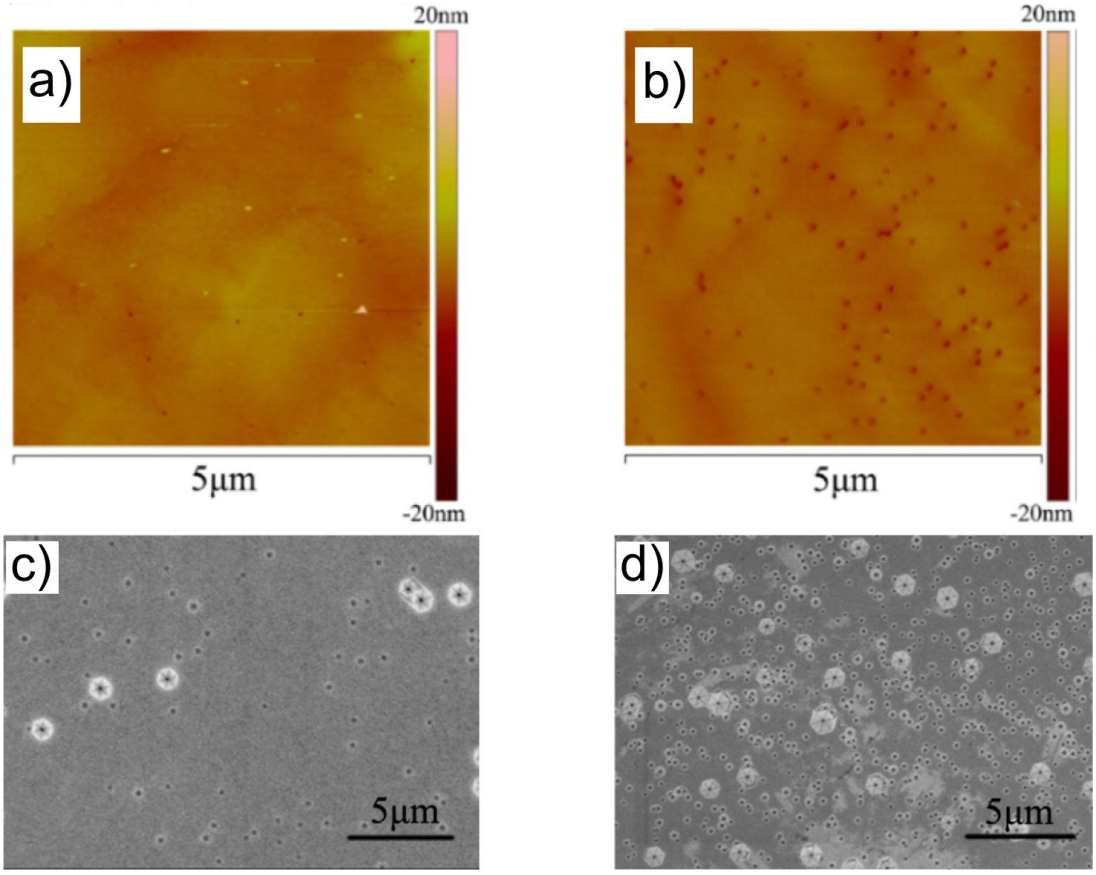

Figure 3.14: AFM images of a) GaN on graphene/GaN/Al_2O_3, b) GaN on GaN/Al_2O_3. SEM images of c) etched GaN on graphene/GaN/Al_2O_3 and d) etched GaN on GaN/Al_2O_3. Retrieved from [40].

quality of GaN crystals using hydride vapour phase epitaxy method. They spin-coated graphene nanosheets on substrate used for epitaxial growth of GaN (5 μm GaN grown on Al_2O_3 by metal-organic CVD). AFM images of GaN substrate with and without graphene nanosheets as the intermediate layer is shown in Fig. 3.14. RMS roughness of deposited GaN on substrate with graphene and without graphene was 0.76 nm and 1.74 nm respectively. They observed very smooth mirror-like surface when using graphene as the buffer layer. Dislocation density in GaN crystals was estimated by etching the samples in KOH-NaOH mixture. In Fig. 3.14 there are shown SEM images of samples after etching. Density of etching pits for GaN on graphene is one order of magnitude lower than on the bare substrate ($1.80 \times 10^7\,\mathrm{cm}^{-2}$ to $1.53 \times 10^8\,\mathrm{cm}^{-2}$). Zhang's group shown pursuing GaN growth methods using graphene has good purpose.

4 Graphene samples preparation

Graphene for our experiments was prepared by CVD method in the furnace built at the Institute of Physical Engineering as the diploma project [34]. A Scheme of the furnace is in Fig. 4.1. Resistance wire is wound around SiO_2 tube and acts as the heating element

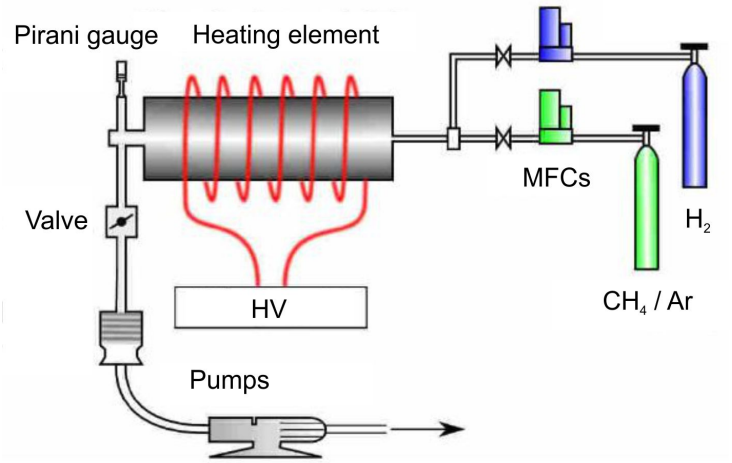

Figure 4.1: Home-made CVD graphene furnace at the Institute of Physical Engineering. Retrieved from [34].

of the furnace. The wire is powered by a high voltage power supply. Gases flow to the chamber through mass flow controllers operated by a LabVIEW programme. Pressure is measured with Pirani gauge (higher vacuum) and with capacitive gauge (lower vacuum). The furnace is pumped out with turbomolecular pump backed by rotary vane pump. Level of vacuum is controlled by the flow control valve. Graphene is grown on copper and then it's transferred to silicon using PMMA as a support layer.

4.1 CVD growth

It is possible to grow two types of graphene layers in the furnace:

- Pollycrystaline graphene
  A whole substrate is covered by graphene layers. Thickness varies across the substrate from monolayer up to fewlayer graphene. Residual PMMA stays on graphene after the transfer to silicon substrate. Fabrication is optimised and therefore relatively easy.

- Single-crystal graphene
  Graphene grows as separated flakes (Fig. 4.2). Only some parts of the substrate contain graphene. Flakes are perfect monolayers, only in the middle there is bilayer, less fewlayers and graphite. Graphene flakes contain just little PMMA residue after the transfer. Fabrication is rather difficult, sensitive and unoptimised yet.

For all the experiments single-crystal graphene was produced for two reasons. Firstly, it has a well defined arrangement compared to a multilayer structure of pollycrystaline graphene. Secondly, single-crystal graphene is much cleaner with very little PMMA residue on top of the layer. Both reasons lead to more reproducible measurements.

The growth process is as follows: at thousand degrees Celsius, methane as a precursor sits on a copper foil and is dissociated. Copper is acting as both the catalyst and the substrate. After dissociation, hydrogen desorbs and carbon atoms migrate on the substrate until connected to other carbon atoms forming a graphene honeycomb lattice.

As the growth substrate, 25 µm thick, commercially available foil was used. The substrate was smoothen by electropolishing where topmost atoms of copper foil (anode) are removed by electrolysis. As electrolyte a mixture of phosporic acid and isopropyl alcohol was used (75 ml H_3PO_4, 50 ml IPA, 100 ml H_2O). Polishing of each side took 1 min at current 0.65 A. Then the foil was inserted into the furnace and it was pumped out. The copper substrate was annealed in Ar/H_2 atmosphere at 8×10^4 Pa. Pressure was maintained with the needle flow control valve. Temperature was set to around 1000 °C and the phase change of copper foil was observed. This was the crucial part. At certain parts, the foil starts to flow and breaks after few minutes. In a vicinity of these part graphene grows. It is important to watch colour change of the foil and at the right moment to lower the temperature. During this process temperature is not so important as the watching of the foil is. Copper was then annealed at lowered temperature for 30 min. The growth of single-crystal graphene flakes was for 55 s at 8 sccm flow of methane. After 10 min, heating was turned off and furnace cooled down. Graphene flakes on copper are visible in optical microscope as unoxidised places as shown in Fig. 4.2.

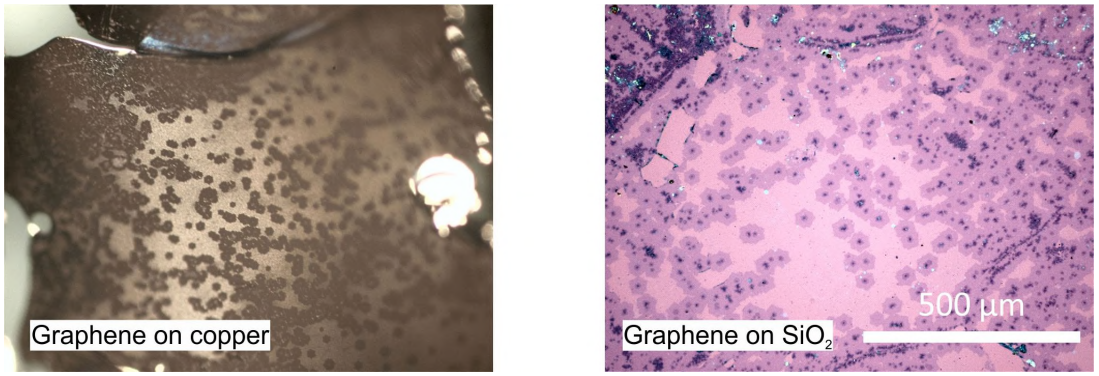

Figure 4.2: Single-crystal graphene in optical microscope. Left: on the copper foil. Right: transferred to 280 nm SiO_2/Si(100).

4.2 Transfer to silicon substrate

After the growth, graphene has to be transferred to a more suitable substrate than the copper foil is. We used $5 \times 17\,\mathrm{mm}^2$ native SiO_2/Si(111) and 280 nm SiO_2/Si(100) substrates. Si is standard material used in semiconductor industry but graphene on Si is practically invisible in optical microscope because it transmits over 97 % of light. This fact makes it more difficult to work with. When we cover Si with right thickness of SiO_2, graphene becomes visible due to an interference. A picture of graphene flakes on 280 nm of SiO_2 is in Fig. 4.2.

To transfer graphene, the Cu foil must be etched away and graphene supported with PMMA. The whole process is as follows:

1. Cover one side of the Cu foil with PMMA using spincoater.

2. Clean excess PMMA from the other side of the foil with acetone.
3. Remove graphene from the other side of the foil with Ar/O_2 plasma.
4. With PMMA on top, put the foil on a surface of strong $Fe(NO_3)_3$ solution to etch the copper foil away.
5. Transfer graphene with PMMA to the surface of deionized water to clean the etchant.
6. Transfer graphene with PMMA to a desired substrate and remove the PMMA layer in acetone.

4.3 Characterisation of grown graphene

Currently, in the CVD furnace at Institute of Physical Engineering we are able to grow single-crystal graphene flakes with the size up to 50 µm. A SEM image of the flakes is in Fig. 4.3. The largest flakes are located in the vicinity of places where the copper foil melted and broke. Hexagonal shape of the flake is from preferential growth related to honeycomb graphene lattice. In the optical microscope picture in Fig. 4.4, there is visible the additional flake in the centre of the large one. Smaller flakes are subsequent graphene layers and graphite as was pointed with Raman spectroscopy.

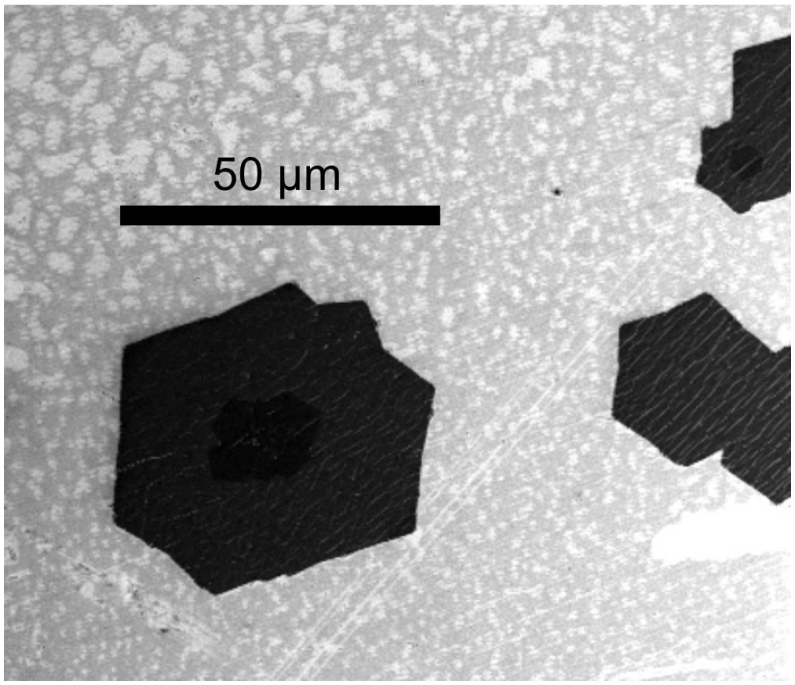

Figure 4.3: SEM image of graphene flakes on 280 nm SiO_2.

Raman spectrum of the monolayer graphene and Raman map of the graphene flakes on the 280 nm SiO_2 is in Fig. 4.4. The map was taken with NTEGRA Spectra microscope from NT-MDT and Raman signal was excited with 532 nm laser. The map has $40 \times 40\,\mathrm{px}^2$ or measured points. Graphs show area counts under graphene characteristic peaks. Defect related D peak in the map (d) shows some adsorbents, most probably PMMA residues on the flakes. Intensity of the G and 2D area counts are homogeneous throughout the most

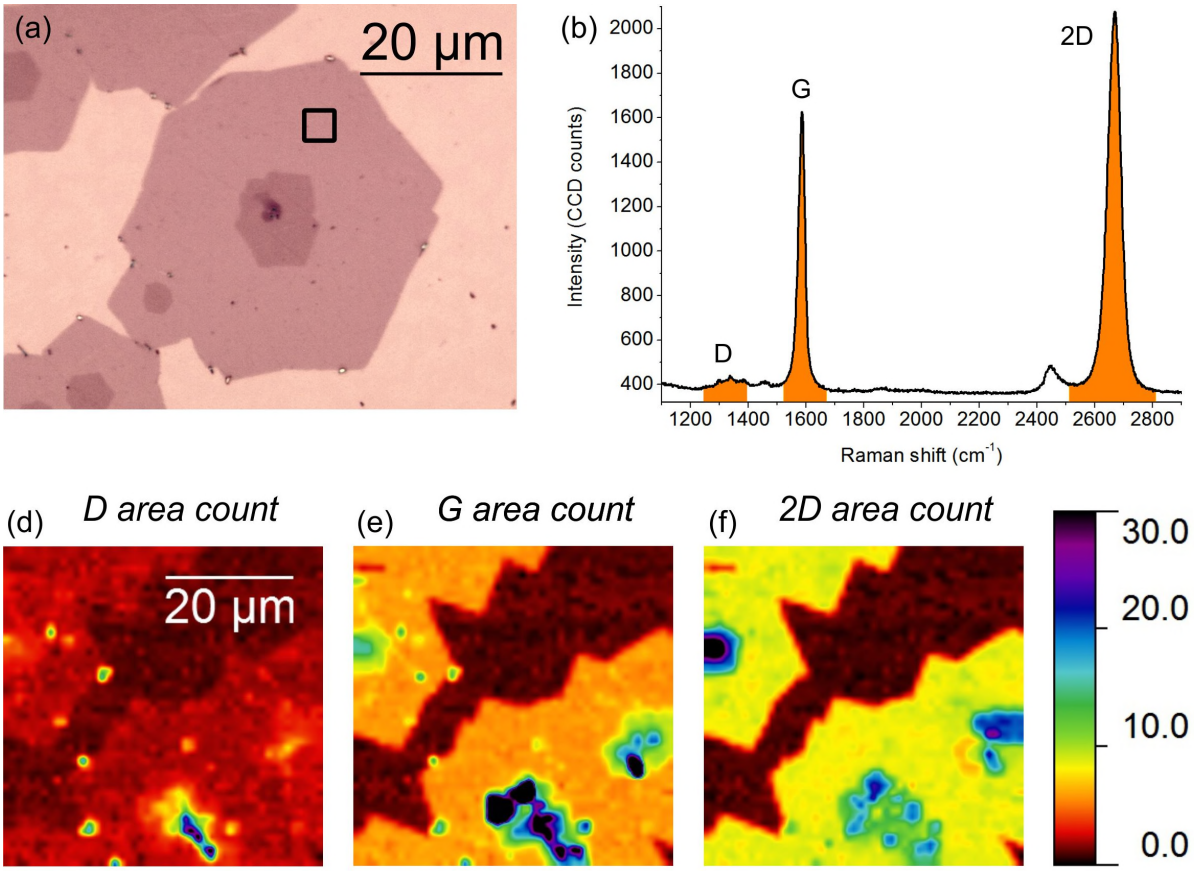

Figure 4.4: Raman spectroscopy of graphene on 280 nm SiO_2/Si(100). (a) optical microscope image of graphene flake. The square marks region from which (b) Raman spectrum was taken. (d)-(f) area counts maps of characteristic graphene peaks. Area ranges are represented by orange regions in (b).

part of the flakes suggesting these parts are monolayer graphene. The highest intensity parts in the G area count map are graphene layers stacked together forming graphite. Optical image shows monolayer flake with darker second layer on top and the darkest part are carbon contaminants or graphite.

PMMA residue ($C_5O_2H_8$) left on graphene after a wet transfer from Cu substrate is possible to minimize by annealing the sample. The boiling point of PMMA in atmosphere is 200 °C. The graphene sample on Si(111) with native SiO_2 layer was annealed in UHV at 400 °C for 2 h. Composition of the sample prior and after annealing was determined by X-ray photoelectron spectroscopy (XPS). In XPS, X-ray beam is used to emit core electrons from elements in the sample. Kinetic energy and number of electrons are detected. Each element has its own characteristic XPS peaks so the sample composition can be determined. A full range spectrum with main peaks labeled is in Fig. 4.5 (a). C1s peaks before and after annealing are in Fig. 4.5 (b) and (c). We observed decrease of carbon-oxygen components from the C1s peak and also we noticed the decrease of the O1s/Si2s ratio from 5.5 to 3.8 due to PMMA evaporation. Native SiO_2 contributes to O1s peak as well. After background subtraction, spectra were fitted in Unifit 2013.

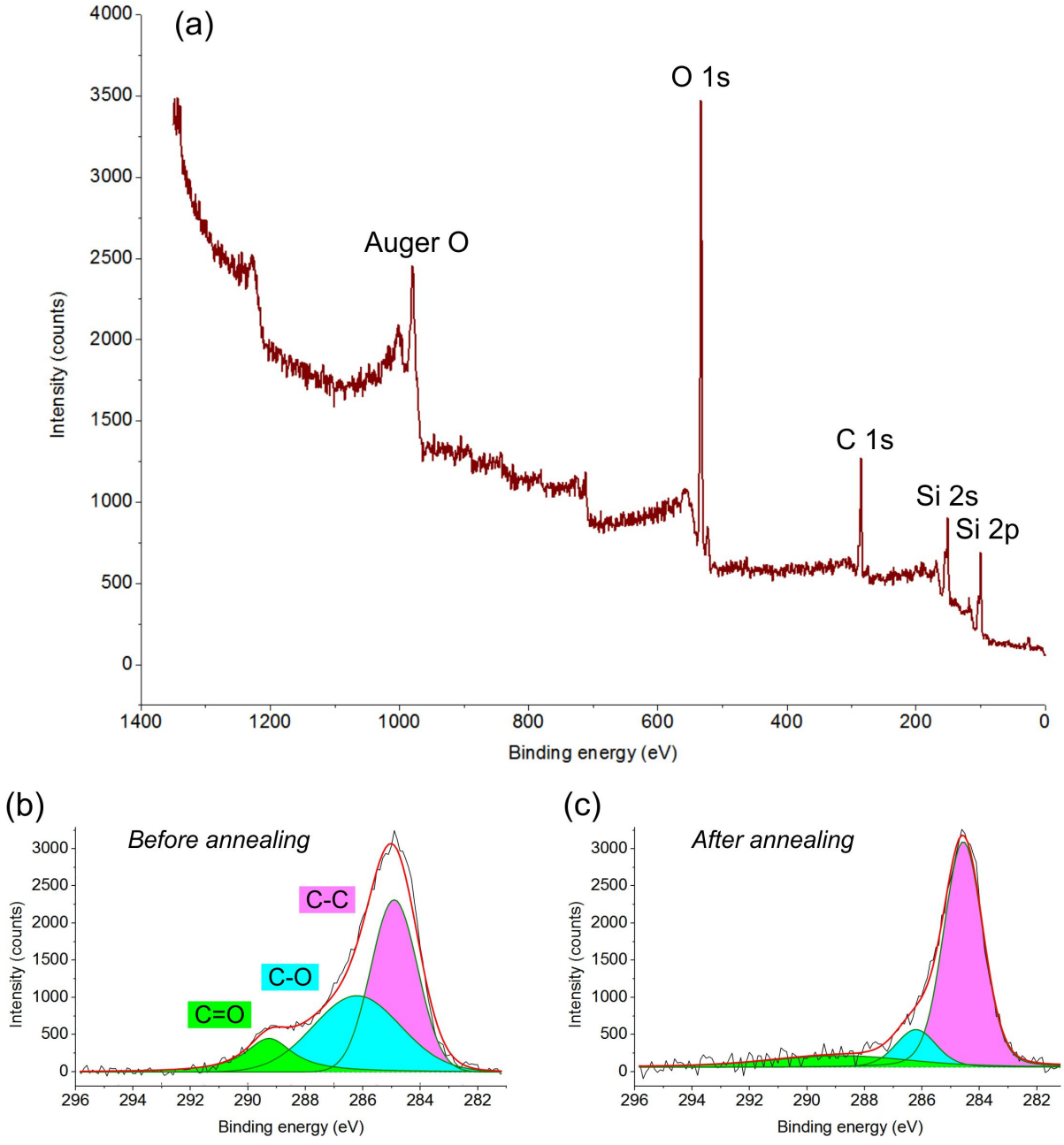

Figure 4.5: XPS of graphene on native SiO_2/Si(111). (a) Full spectrum with characteristic peaks. (b) and (c) are C1s peaks taken before and after annealing. Black curves are measured data, red curves are the sum of fitted components.

5 Ga depositions on graphene and SiO_2/Si

Two Ga deposition experiments were carried out on CVD graphene flakes. In the first one, substrate temperature was variable parameter. The second experiment was done with sample kept at 300 °C and the deposition time was changing.

5.1 Experimental details

Samples were annealed prior to Ga depositons at 440 °C in UHV either by heating the sample directly with electrical current or by pyrolitic boron nitride (PBN) sample heating element at which the sample was fixed. Ga was deposited using Omicron EM3 effussion cell. Molybdenum crucible in the cell is heated to around 800 °C by electron current 26 mA emitted from heated tungsten filament. Electrons are accelerated towards the crucible by potential difference 800 V applied between the crucible and the filament. Amount of evaporated Ga is measured as Ga flux current from ionised Ga atoms. Ga flux was kept constant at 78 nA which corresponds to approximately 0.2 ML/min. Base pressure of the deposition chamber was 10^{-7} Pa.

5.2 Ga deposition with the sample temperature as a parameter

We deposited Ga on three Si(111) samples with graphene flakes on it. A native layer of SiO_2 on silicon was present. Depositions were done at room temperature (25 °C), at 400 °C and again at 400 °C but in this case, the sample was kept at 400 °C for 30 more minutes after the deposition ended (we will tag this deposition as 400 °C + 30 min from this point on). Deposition time for each sample was 1 h. Samples were heated directly with current and temperature was measured by optical pyrometer with emissivity 0.7.

SEM and AFM topography image overwievs of the samples after depositions are in Fig. 5.1. SEM images were measured with TESCAN Lyra3 and AFM scans were taken with Bruker Dimension Icon in the ScanAsyst mode. Each of the images include both graphene flake part and SiO_2/Si part of the sample for comparision. Left side of each image shows graphene and in the right part there is SiO_2/Si. Most Ga particles is observed on the 25 °C sample for both graphene and SiO_2/Si. Size of Ga particles is much increased at 400 ° because Ga atoms have more thermal energy from the hot substrate. Hence, particles migrate on the surface until they meet each other and coalesce into bigger islands. A preferential configuration of Ga on graphene has origin in the copper foil production process used for graphene growth. Rolling cylinder for thinning copper foil has small grooves on it which are imprinted to the foil. Graphene is wrinkled at these grooves and Ga tends to stick there. When the copper foil is partially melted, grooves dissapear. So we see the pattern only on some flakes grown on unmelted parts of the copper foil. On 400 °C + 30 min sample, Ga coalesced into big islands just the same way like on the previous sample except in this case, sample was left for 30 more minutes at elevated temperature

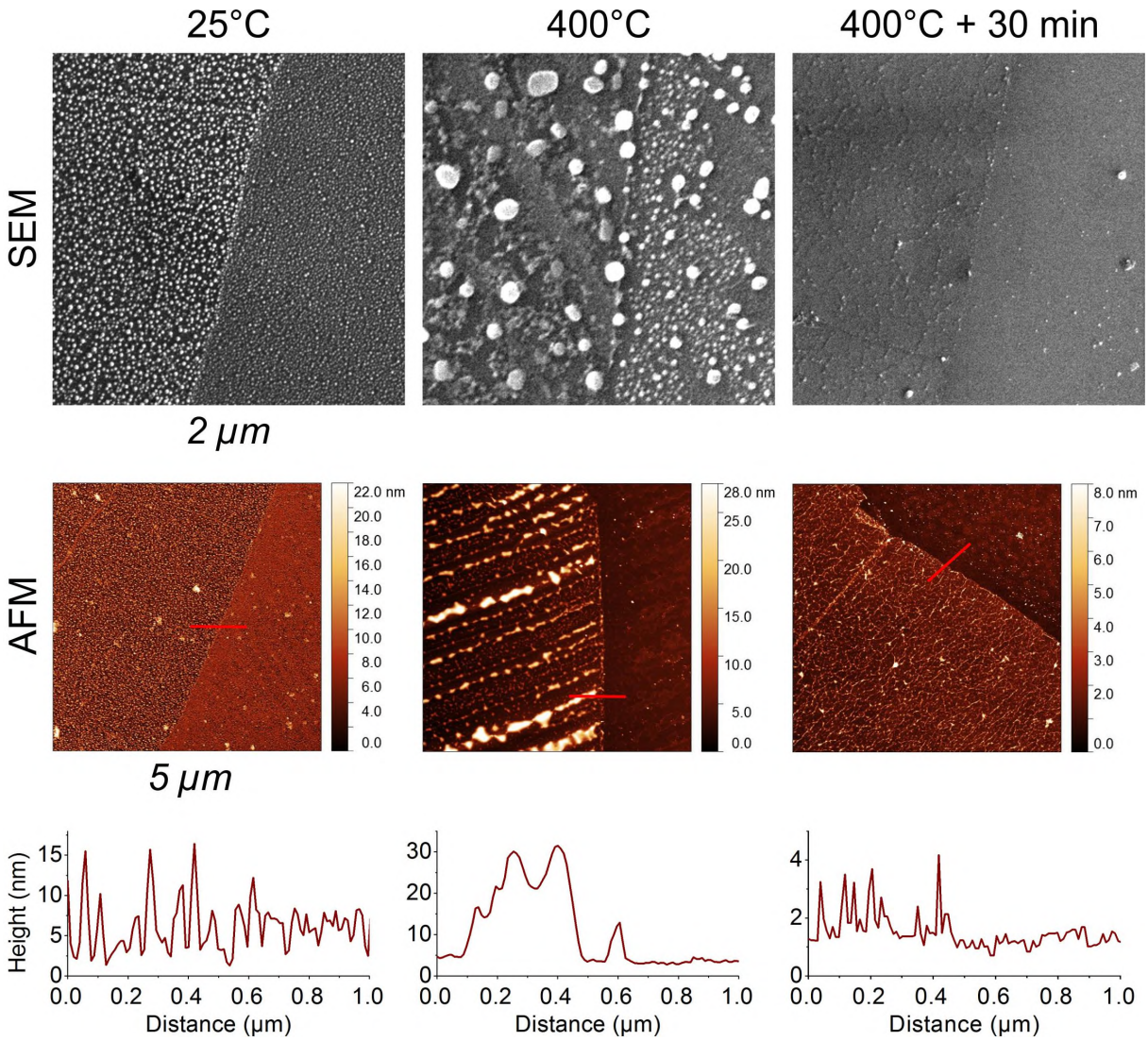

Figure 5.1: SEM and AFM overview of Ga deposited samples. Left part of each image is graphene, right part is SiO_2/Si. Height profiles are along the red lines below each of the AFM images.

after deposition ended. Therefore, the balance between adsorption and desorption was disturbed and sample surface was left with very little Ga.

XPS spectra (Fig. 5.2) were taken in the UHV apparatus complex right after deposition, without a sample exposition to the atmosphere. In the XPS graph, we can see increasing Ga peaks and decreasing Si peaks from pristine graphene up to 25 °C sample that is in congruence with SEM and AFM images in Fig. 5.1. Sample 'before deposition' was annealed in the Ga deposition chamber, therefore we see Ga trace peaks in the spectrum. The peak ratio Ga2p$_{3/2}$/Si2s for all the Ga deposited samples is in Tab. 5.1. The highest ratio is for 25 °C because this sample is highly Ga covered even on SiO_2/Si area in contrast with other samples where Ga coverage on SiO_2/Si regions is much lower.

Detailed AFM images of samples revealing Ga structures for both graphene and SiO_2/Si areas are in Fig. 5.3. We notice quite a variation in the topographies. On 25 °C sample, Ga forms spheres (although contact angle is unknown). Sphere distributions are displayed as histograms below AFM scans. Distributions were obtained from the AFM

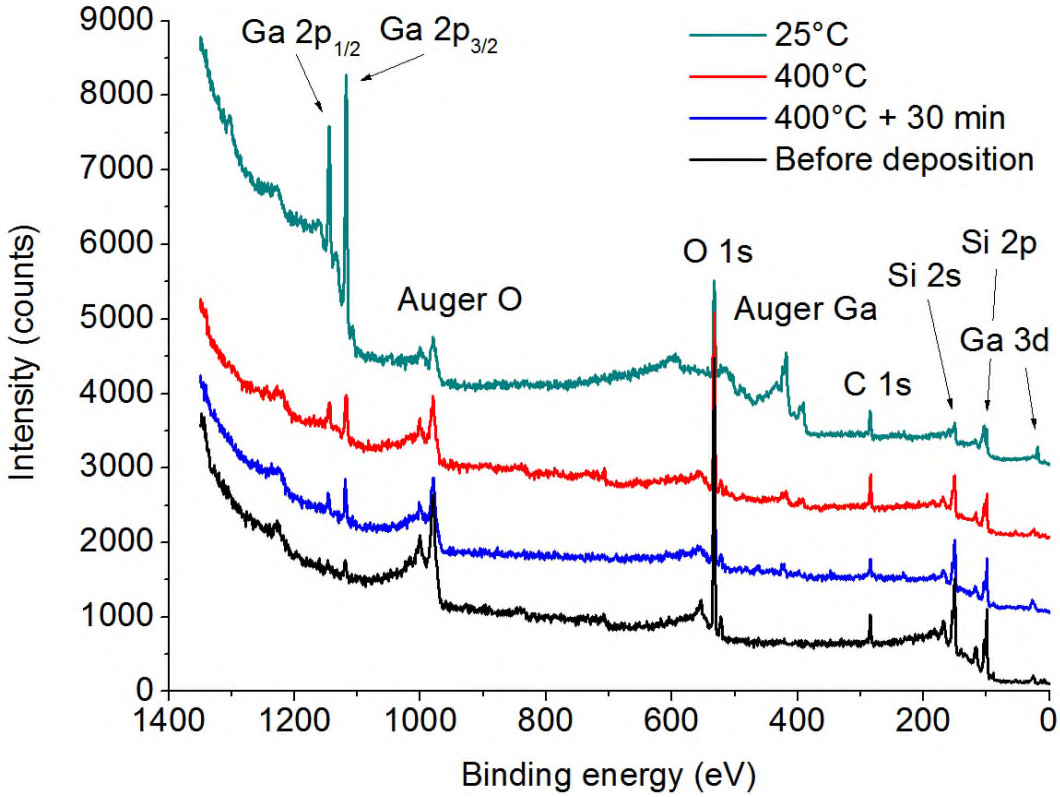

Figure 5.2: XPS spectra before and after Ga depositions on graphene/Si(111) with the native SiO_2 layer. Most intense peaks are labeled. Data curves are offset for clarity.

scan using software Gwyddion and combination of its functions *Mark by Segmentation* and *Mark by Treshold* [29]. Identified small sized particles were filtered out as a noise. A size of particles and the total volume are in reality smaller because AFM topography signal is convolution of the sample topography and the scanning AFM probe. Qualitatively, the sphere distribution is very similar for both graphene and SiO_2/Si. The size of spheres is bigger for graphene than for SiO_2/Si, the total Ga surface coverage is the same though. Ga particles on graphene diffuse easier and coalesce more, forming bigger spheres. Ga deposited volume on graphene is higher than on SiO_2/Si which says graphene has higher sticking coefficient (the ratio of the number of atoms that adsorb to a surface to the total number of impinging atoms) than SiO_2/Si. Deposited volume is in units of monolayer (1 Ga ML = 0.45 nm). Total Ga impinging volume for 1 h is about 12 ML. With AFM we measured 8.4 ML of Ga on graphene and 6.2 ML on SiO_2/Si. A rough estimation is that around 70 % (50 %) of impinging Ga atoms sticked to the graphene flake (Si substrate).

Table 5.1: XPS Ga and Si peaks ratio for a comparision of the deposited Ga amount.

	400 °C + 30 min	400 °	25 °C
$Ga2p_{3/2}$/Si2s ratio	0.88	1.12	15

Topography of the 400 °C sample is different. Ga on graphene forms not perfect spheres but rather coalesce into big islands $50 - 100$ nm in size. Deposited volume for graphene and for SiO_2/Si is 5 ML and 0.2 ML respectively. SiO_2/Si is covered with Ga only little because Ga desorption is much higher for SiO_2/Si than for graphene at 400 °C. Elevated

temperature causes Ga atoms to desorb with higher probability as when the sample is at RT.

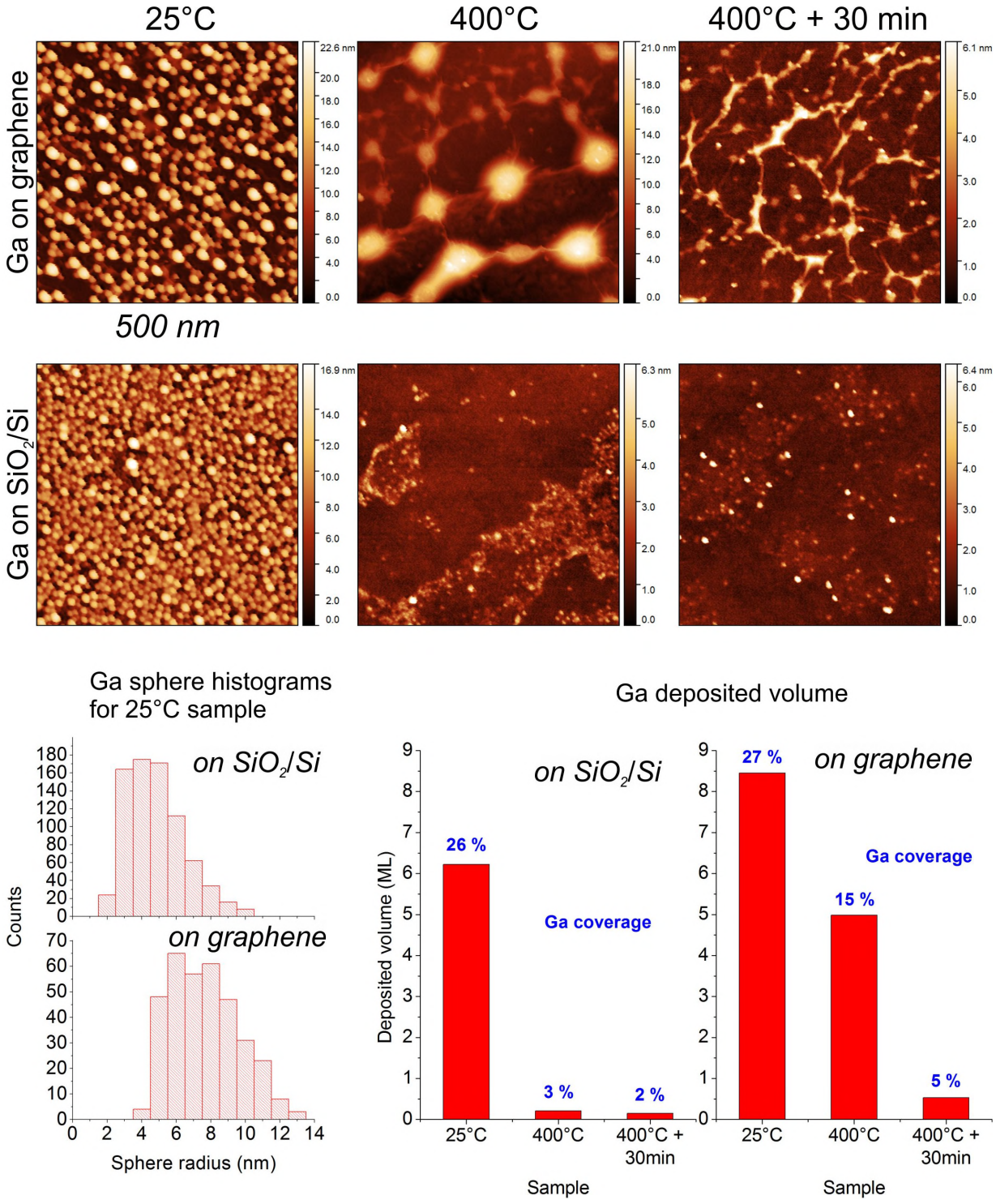

Figure 5.3: Detailed AFM scans of samples after depositions. Graphs on the left show Ga sphere histograms for 25 °C. Graphs in the middle and on the right show total Ga volume on the samples in monolayers after depositions as measured with AFM for both graphene and SiO_2/Si(111) parts of the sample. Ga coverage is percentage of the scanned window surface covered with Ga determined manually with Gwyddion software.

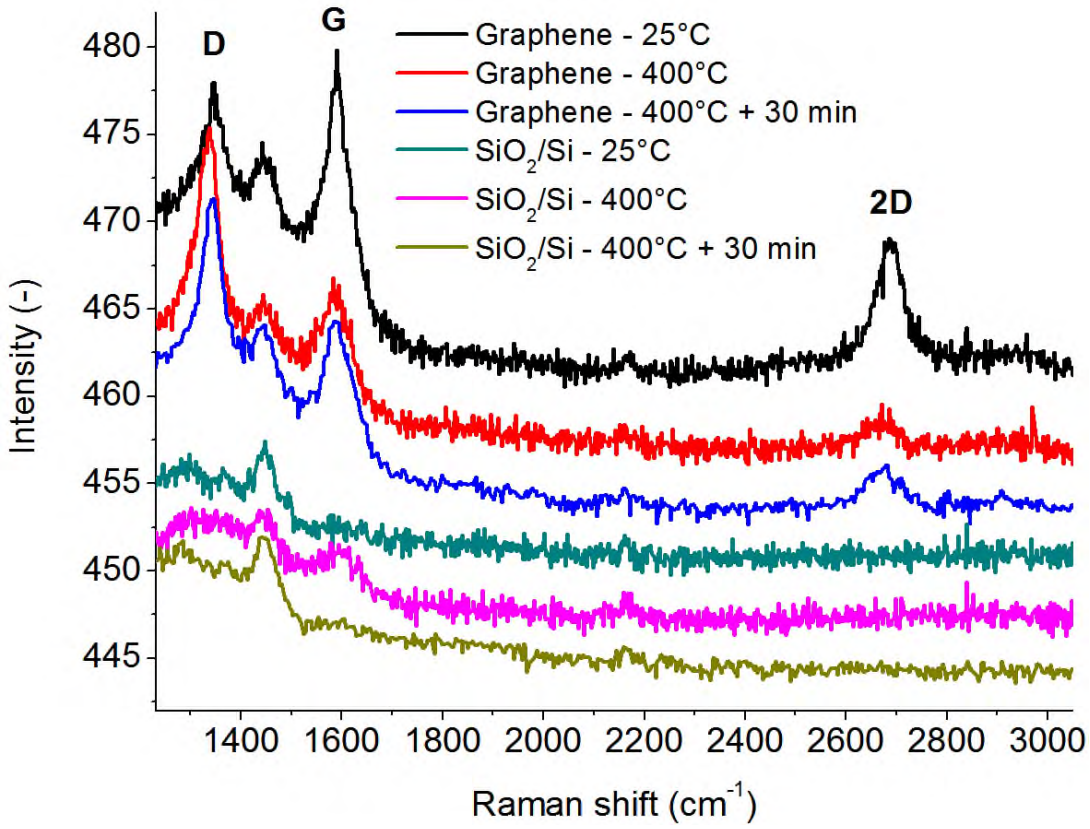

Figure 5.4: Raman spectra of Ga on graphene and Ga on native SiO_2 as a background. Spectra are equidistantly offset. Unlabeled peak around 1450 cm^{-1} is probably related to silicon.

When a sample is left for 30 more minutes at 400 °C after the deposition, more Ga is desorbed. A desorption rate is exponential so much higher fraction of Ga is desorbed from graphene than from SiO_2/Si. When comparing the image of 400 °C and 400 °C + 30 min we see the latter has the same structure as the former with highly reduced volume of the Ga islands. Ga is mostly desorbed from large-island regions where Ga has the highest desorption probability. The Ga thread pattern is reduced but still kept.

Next, we wanted to see how Raman spectra evolved after gallium deposition. Spectra were measured with TESCAN RISE microscope which implements Confocal Raman microscope from WITec and GAIA3 GMU scanning electron microscope from TESCAN into one device. Spectra of samples in Fig. 5.4 were taken with 532 nm excitation laser operating at 30 mW. First look at the spectrum reveals the D peak which occurs when graphene is defected or has adsorbates on it which change sp^2 carbon hybridisation into sp^3. Even though Ga does not interact with graphene chemically very well and what is more, restores graphene structure at the Ga/graphene interface, it still introduces some defects. A height of the D peak is amplified by Raman enhancement and does not correspond to such high density of defects. The D peak is higher for both 400 °C samples (intensities 9) than for 25 °C (intensity 6) as measured from a baseline of each curve. So the height of the D peak is not proportional to volume of Ga on graphene. Graphene G and 2D peaks are enhanced the most for RT sample. This corresponds to highest coverage of Ga on the sample. Mechanisms for Raman enhancement on metallic particles on graphene are two – doping from metal or electromagnetic effects (plasmonics). Both mechanism could

contribute to the observed enhancement. By studying further depositions, we will find more.

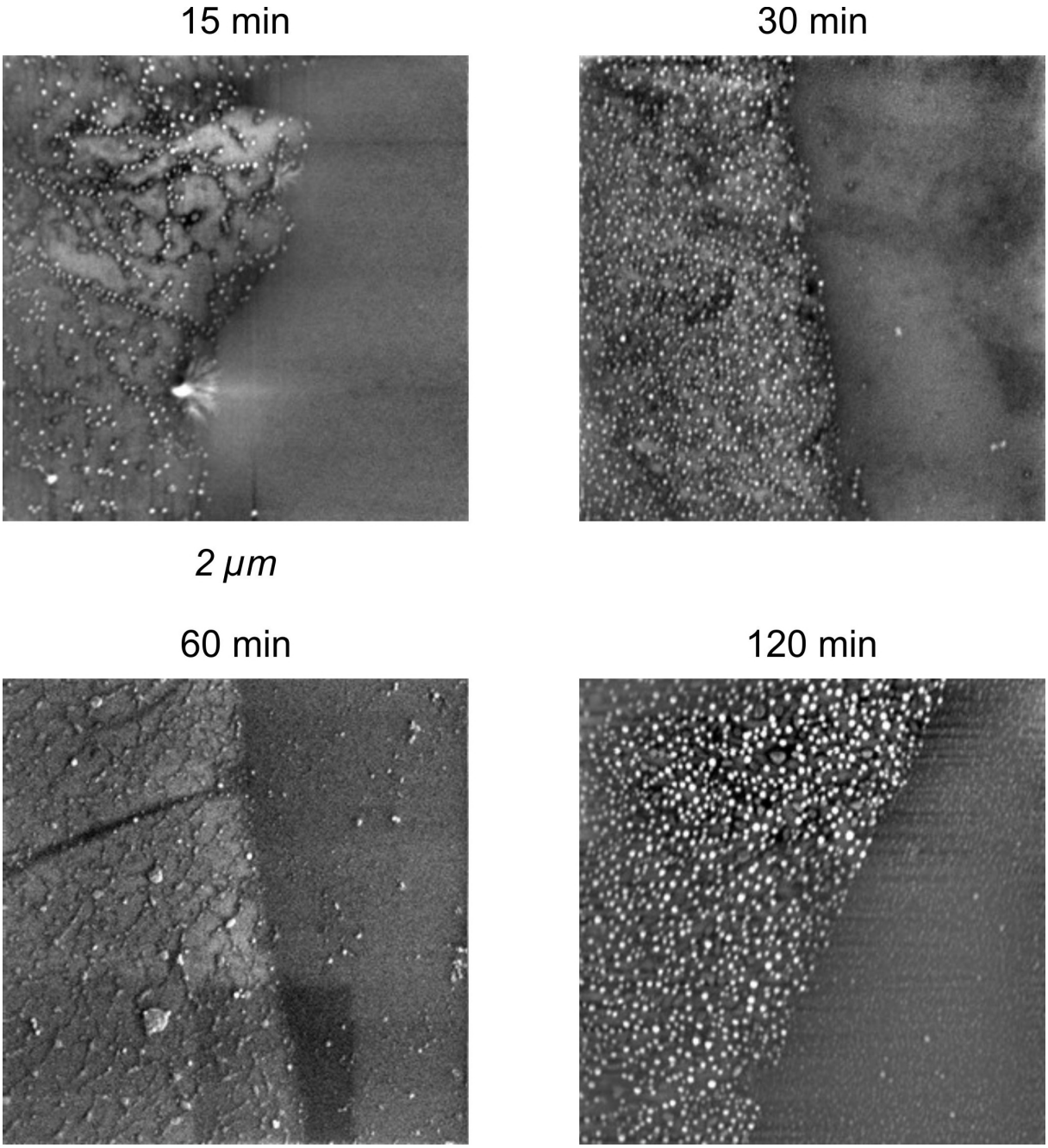

Figure 5.5: SEM images of graphene/SiO_2 samples with deposited Ga for 15, 30, 60 and 120 min. Samples were at 300 °C during the deposition. In each picture, graphene flake is on the left and SiO_2 is on the right.

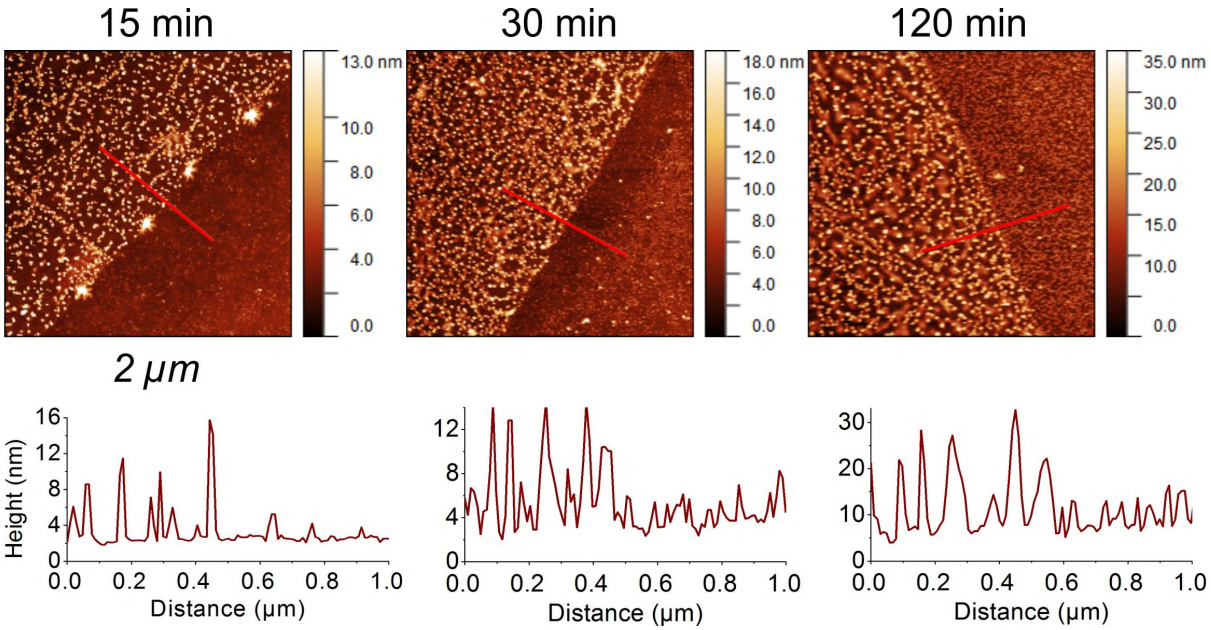

Figure 5.6: Large scale AFM images of Ga deposited on graphene/SiO_2 at 300 °C. Left parts are graphene, regions on the right are SiO_2. Four big bright spots on the graphene edge in the left image are PMMA residues. Deposition times are above the images for each sample. Height profiles along the red lines are below AFM images. Scan sizes are 2 μm.

5.3 Ga deposition with the deposition time as a parameter

Graphene on Si with a few nm of native SiO_2 is practically invisible for detection in optical microscopes. Also in Raman spectroscopy, the spectrum aquisition requires more laser power which can damage graphene. For these reasons, CVD graphene was transferred to Si(100) with thermally grown 280 nm SiO_2 layer in the following experiment. A multiple interference of light reflected from air/graphene/SiO_2/Si interfaces allows us to see graphene very easily in optical microscope using white light.

In the following experiment, we deposited Ga on graphene/SiO_2 samples held at 300 °C during the deposition. Samples were deposited for 15, 30, 60 and 120 min. All the samples were heated with PBN heating element except 60 min sample which was heated directly with current due to a logistic reason. Temperature of directly heated sample was measured with optical pyrometer. The PBN heating element is well calibrated and temperature is controlled with current passing through it. An accuracy of the pyrometer is lower than of pyrolitic BN and as the result Ga deposited structure is different. Therefore, except a general Raman measurement, 60 min sample was processed separately.

SEM scans of samples after depositions are in Fig. 5.5. Images cover both graphene flake (left part) and SiO_2 (right part of each image). Ga forms spheres on every sample except 60 min sample which was heated differently than other samples during the Ga deposition. On the 15 min sample, the pattern formed by spheres copies the pattern of cracks occuring on a pristine graphene flake. Cracks and defects are preferential sites for Ga to stick after undergoing a surface diffusion. The pattern vanishes and spheres become distributed more randomly as the Ga coverage increases with increased deposition time.

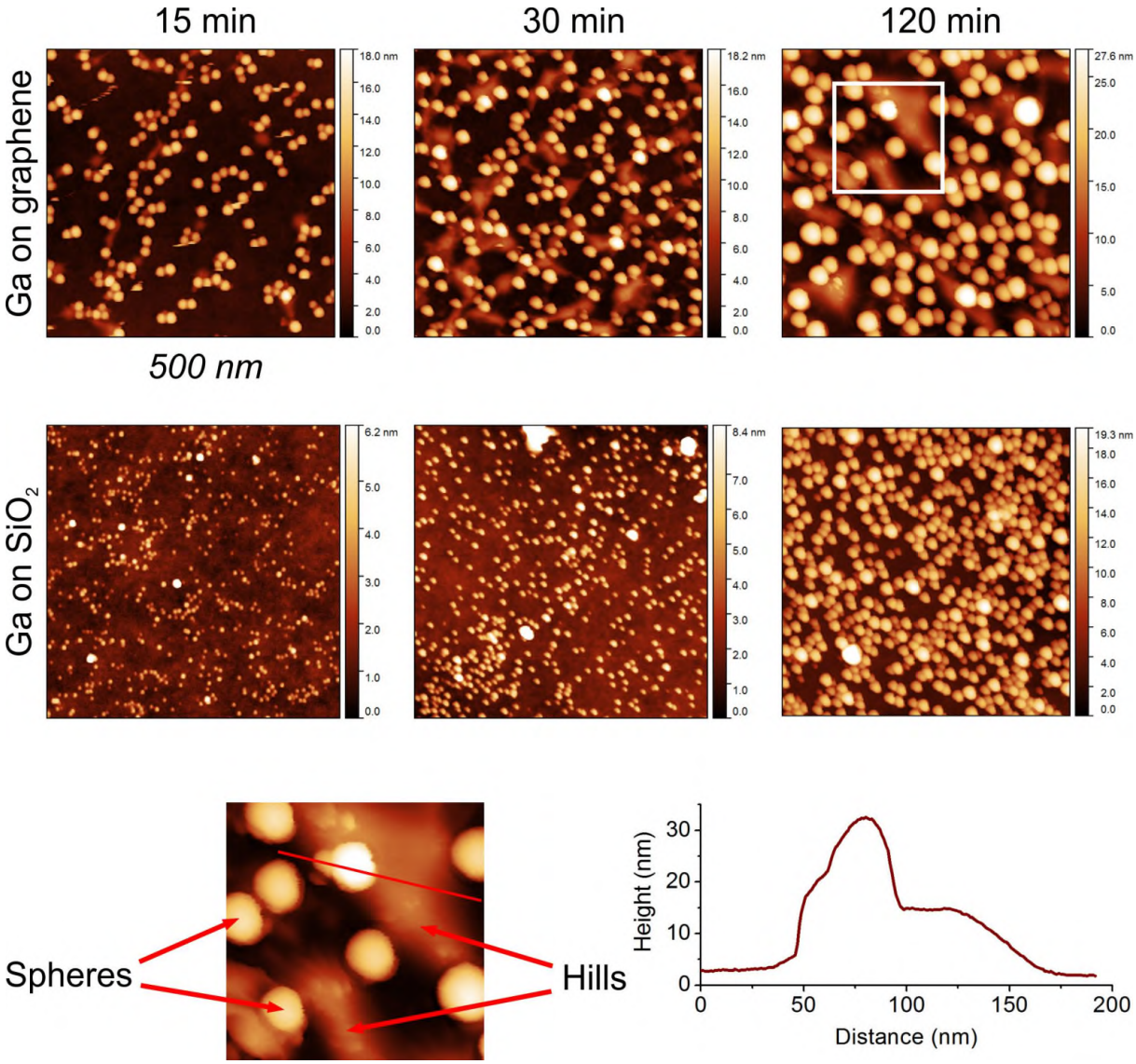

Figure 5.7: Detailed AFM scans of Ga deposited on graphene and SiO_2 at 300 °C. Image at the bottom is zoomed area bounded by white square and shows two types of clusters formed - spheres and hills. The graph is plot along the red line.

An increased size of spheres on the 120 min sample is the result of prolonged diffusion time of Ga clusters due to the long deposition and their coalescence into larger spheres.

Large scale AFM images for overview in Fig. 5.6 are consistent with SEM images. Ga coverage is less for 15 min sample and approximately same for 30 and 120 min samples. Big bright spots in the images are PMMA residues from graphene transfer. Ga coverage is higher on graphene than on SiO_2 implying that Ga sticks better to graphene. For more topographic information we performed detailed 500 nm AFM scans for both graphene flake and SiO_2 part of the samples. Scan images are in Fig. 5.7. In the scans we observe spherical Ga shapes even on SiO_2, much smaller though. The size and coverage increase with deposition time. The same is true for graphene flakes. Apart from spherical shapes, Ga forms also another structure on graphene – 'hills', which are connected to form Ga threads on the surface. The height of hills is about half less than that of spheres. The reason for hills formation is graphene has perfectly defined surface only in theory yet. Due

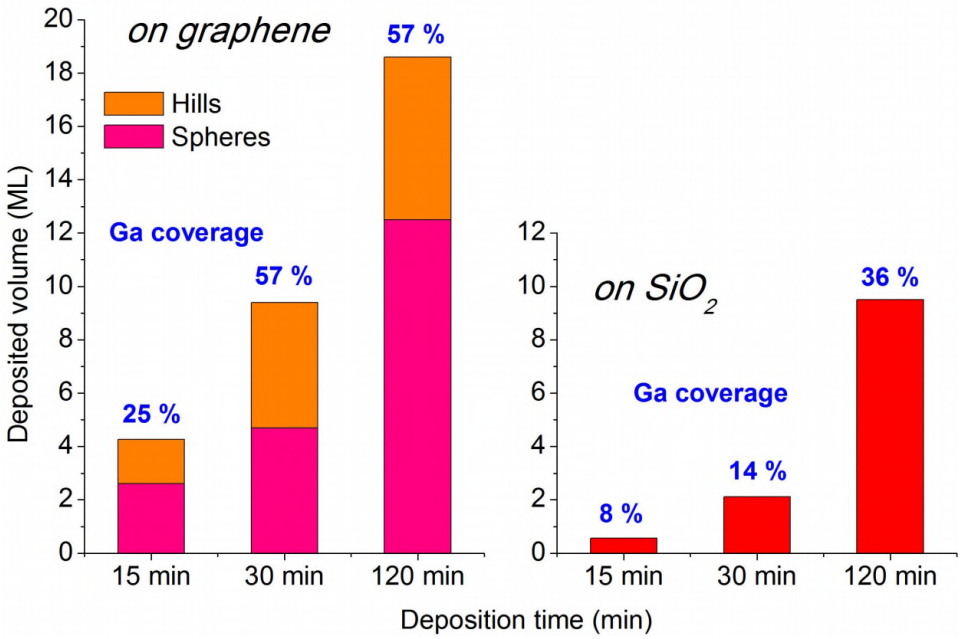

Figure 5.8: Ga deposited volume as obtained from AFM scans together with information about Ga surface coverage.

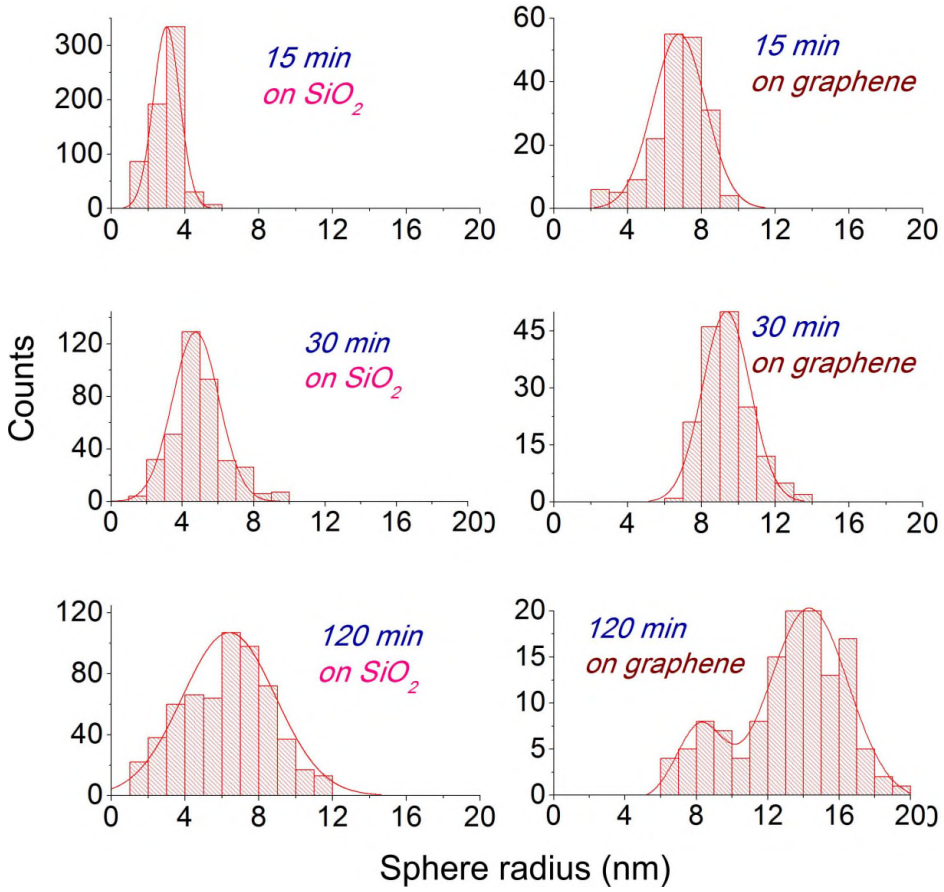

Figure 5.9: Distributions of Ga spheres obtained from AFM scans. Width of the bins is 1 nm. Curves are fitted Gaussians. All the histograms have normal distribution except 120 min graphene histogram which has binormal distribution.

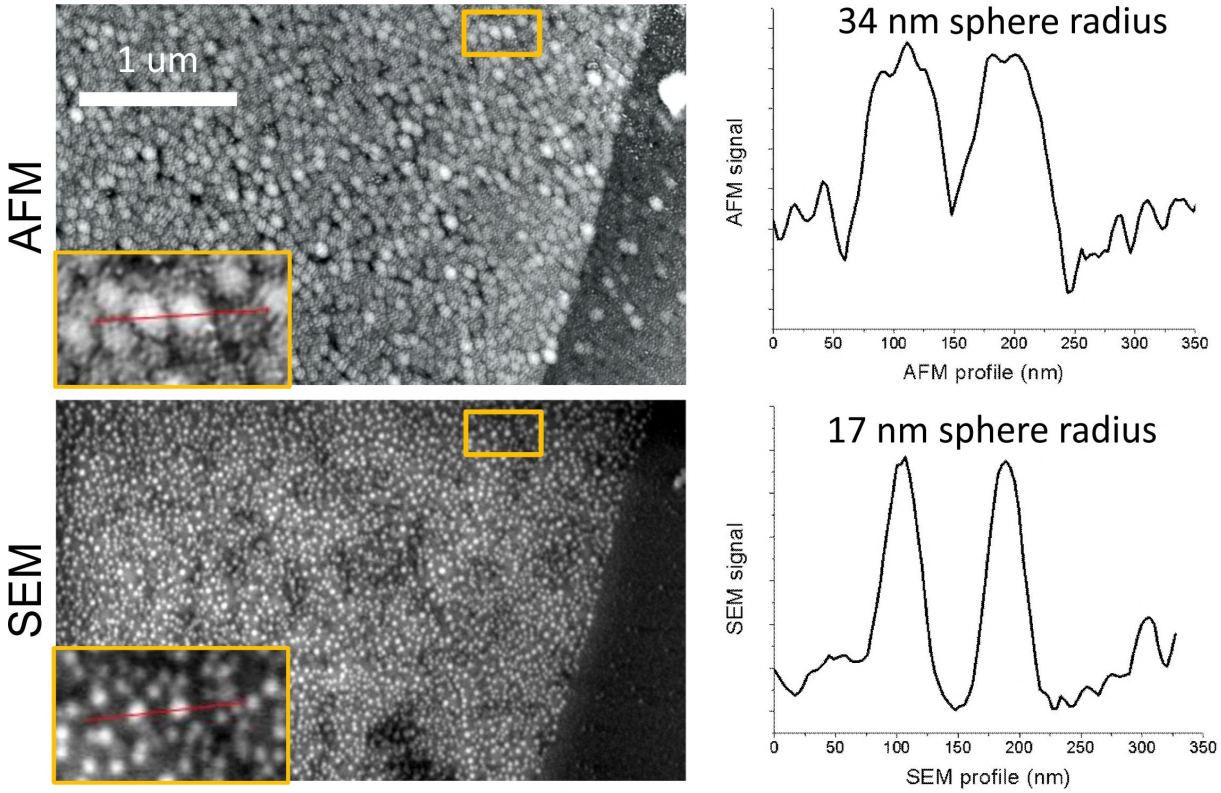

Figure 5.10: Information comparision obtained with AFM and SEM measured at the same place on the 120 min sample. Convolution of the AFM tip and the sample doubles diameter of the spheres. AFM image was scanned in the tapping mode with the tip apex radius 10 nm. Profiles of both signals are along the red lines in each image.

to even small PMMA residues and cracks, graphene is more rough than SiO_2 and thus, Ga has more available sites to stick at. Roughness of graphene causes sphere shapes are not energetically the most favourable everywhere and that's why hills are formed at some places.

The estimation of Ga deposited volume and coverage was done in Gwyddion software. As expected, coverage and volume are higher for graphene and increase with depositon time for both graphene and SiO_2. Hills on graphene form quarter to half of total deposited volume. The rest is filled with spheres. Ga surface coverage on graphene for 30 and 120 min samples is the same, latter contains higher volume. Coverage uncertainty is $\pm 10\,\%$.

AFM method for determining deposited volume is not exact due to convolution of the tip with the scanned sample surface and we estimate volume to be up to 30–40 % higher. Nevertheless, the comparision between samples of a similar structure as our samples are is quite accurate. Concrete example of the convolution between the AFM tip and sample is shown in Fig. 5.10. AFM was measured in the tapping mode with the tip apex radius 10 nm. Graphene sample with Ga on top was scanned at exactly same place with two SPM techniques – SEM and AFM. While SEM image shows morphology precisely, AFM topography is influenced by convolution. Profiles along couple of Ga spheres show that AFM scan can double the value of real sphere size. Even though the SEM and AFM signals are of different nature, both are used for obtaining information about sample

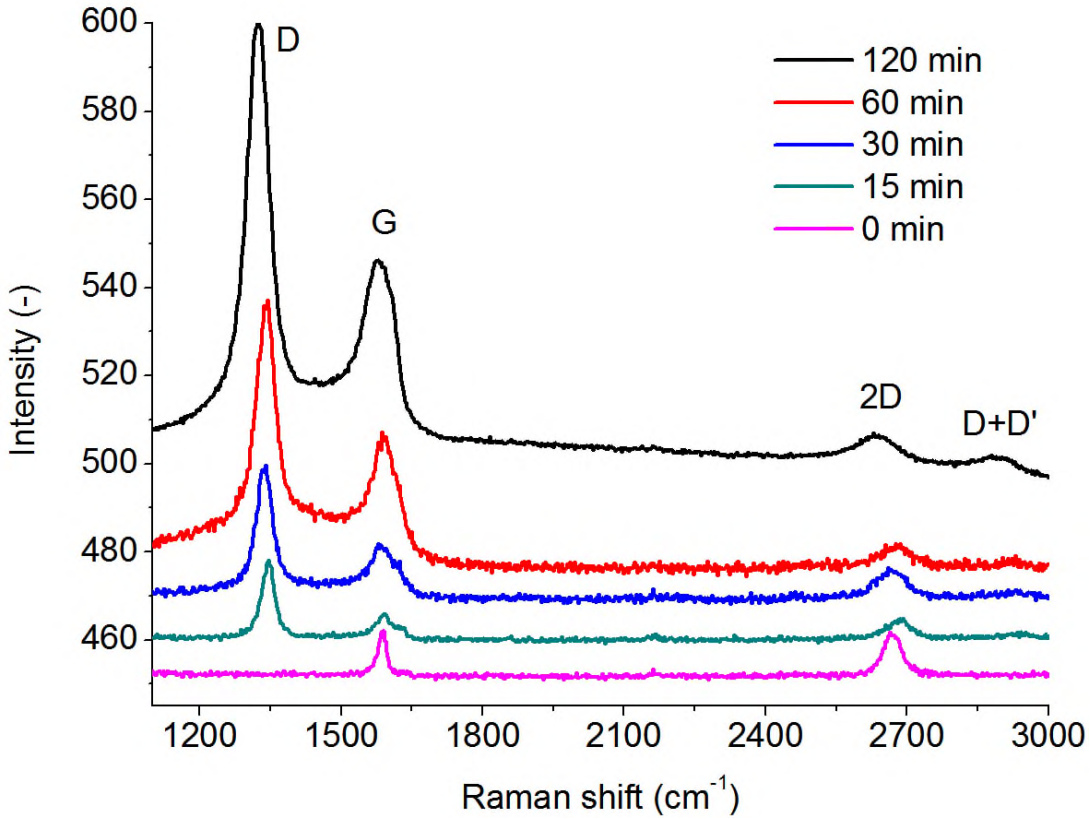

Figure 5.11: Raman spectra of graphene on 280 nm SiO_2 with deposited Ga for various deposition times. 0 min is for graphene without Ga. Spectra are offset for clarity.

structure and output can give us useful insight about the sample, what we see is nothing more than interaction of the measuring device with the object we are measuring.

Detailed AFM scans from Fig. 5.7 were used for determining of sphere distributions on the samples that is in Fig. 5.9. An average radius of spheres is higher for graphene than for SiO_2 and the radius dispersion tends to increase with the deposition time. Distributions of sphere radii is normal except for 120 min graphene where is binormal. Sphere radius data were divided into 1 nm wide bins.

Raman spectra of samples are in Fig. 5.11. Spectra were excited with 532 nm laser of power 7 mW. After deposititon, D peak emerges. Spectra are enhanced with deposition time, predominantly region with D and G peaks. Also, D and G peaks tend to move to lower wavenumbers. 2D peak broadens and both its position and intensity have no clear correlation with deposition time. This can be due to the facts, that on the one hand, Ga amplifies the spectrum and on the other hand it introduces defects and thus lowers 2D intensity. Combining of the two effects, the intensity of the 2D peak does not change much. An enhancement of spectra can be of plasmonic nature when incoming excitation laser intensity is amplyfied in the specific regios by metallic Ga spheres.

Closer look at the G peaks after the deposition reveals they have shoulders on the right side. Broadened G peaks hide a second peak of lower intensity. In Fig. 5.12 we fitted the broad G peaks after background subtraction with two Lorentzians. Smaller fitted peak has position around 1610 cm^{-1} and was identified as the D' peak related to defected graphene. In Fig. 5.13 fitted peak positions are plotted against the Ga sphere size. Sizes of the spheres are maxima of the histograms in Fig. 5.8. Peaks positions decrease with

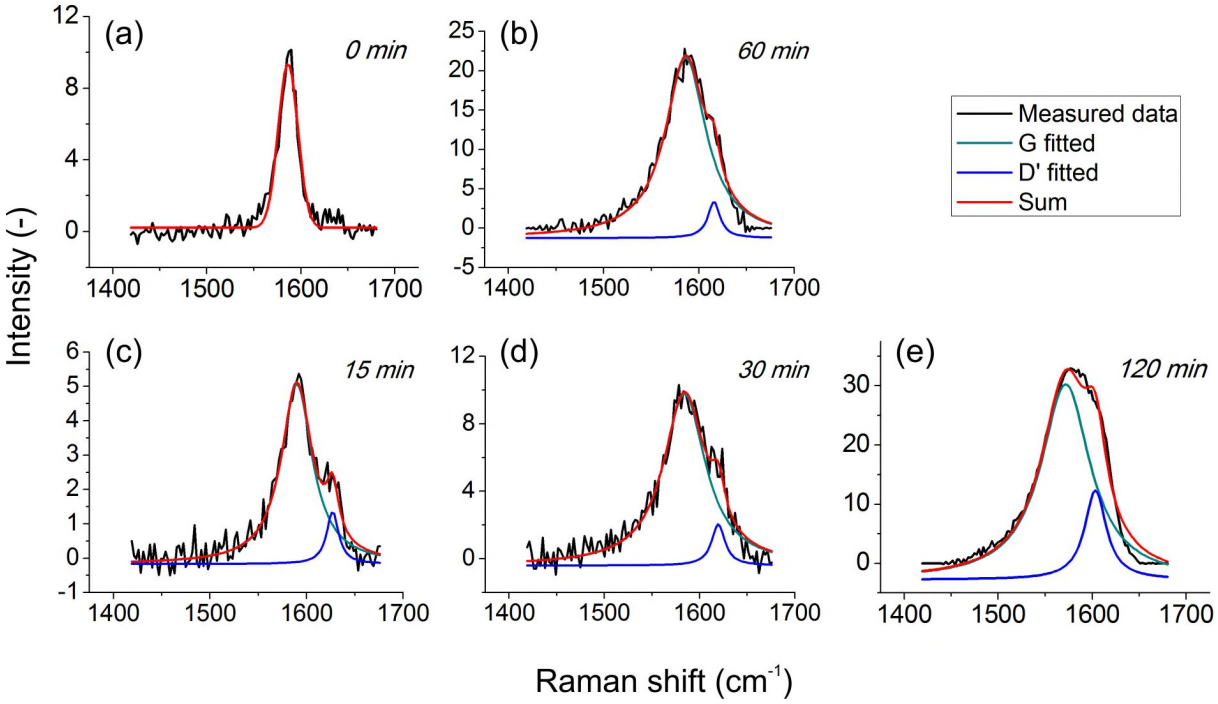

Figure 5.12: Fitted broad G peaks from Fig. 5.11. Baseline was subtracted and data were fitted with two Lorentzians.

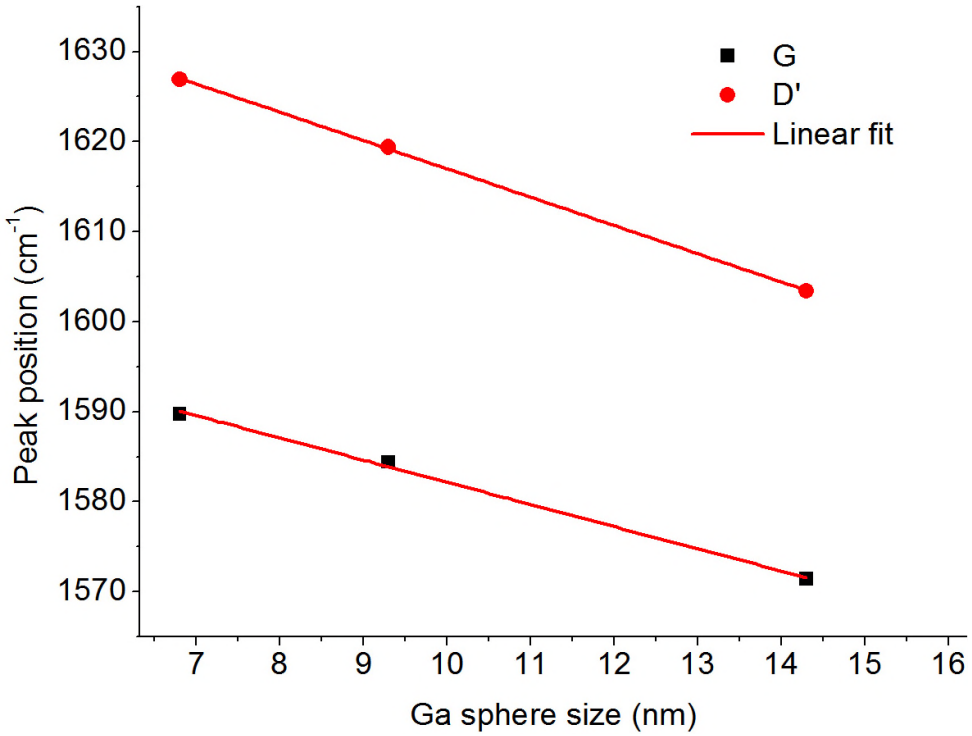

Figure 5.13: Fitted peak positions versus Ga sphere size as obtained from histograms in Fig. 5.8.

increasing sphere size. According to [27], Raman peaks of graphene behave this way when the lattice is under strain. They shift to lower wavenumbers when the strain is tensile and to higher wavenumbers when the strain is compressive. A possible explanation for

peak shifts is Ga spheres cause higher tensile strain of the graphene lattice and the strain increases with the Ga sphere size.

To conclude, Ga sticks better and forms larger spheres on graphene than on SiO_2. Sphere distributions are normal. A presence of Ga on the graphene surface introduces defects and graphene Raman peaks related to defects (D,D') emerge. Also, Raman spectra are enhanced and peaks are shifted to lower wavenumbers. Shifts can be caused by tensile strain of graphene lattice by Ga islands.

6 Raman enhancement by individual Ga islands

Gallium formed large islands visible even in optical microscope (Fig. 6.1 (a) and (b)) on the sample heated during the deposition to 300 °C directly by electric current. Islands are of two types. Spheres with 70-100 nm diameter, visible as the bright spots in Fig. 6.1 (d) and (e) and hills, with approximately half of the sphere height but larger in projected area. Zoomed AFM topography of the hill is in (f). Profiles of the hill and sphere is in (g) part of Figure. Besides spheres and hills, whole surface is covered by Ga threads 6 nm high as shown in the 60 min sample in Fig. 5.5.

To be sure whether hills and spheres are really composed of Ga, we performed Energy-dispersive X-ray spectroscopy (EDS) measurement. EDS is an analytical technique utilising electron beam as the probe and X-rays as the signal to obtain a chemical composition of the sample. A penetration depth is a few µm depending on the electron beam acceleration voltage and atomic number of the sample.

We used EDS from EDAX mounted in scanning electron microscope FEI Verios 460L located at CEITEC. Both island structures consist of Ga as seen in the spectra in Fig. 6.2.

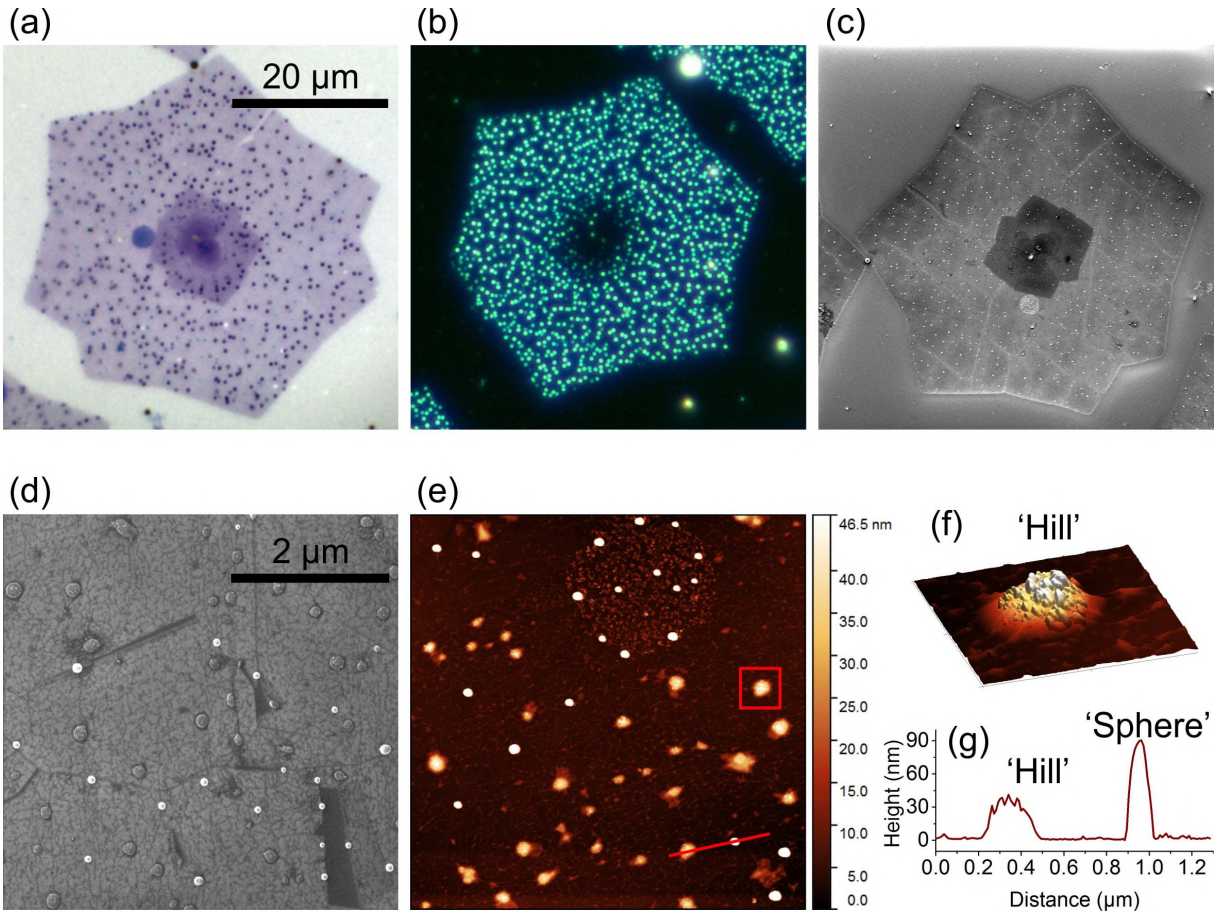

Figure 6.1: Images of sample with large Ga islands. Deposited for 60 min at 300 °C. Optical microscope: (a) bright field and (b) dark field. (c) and (d) SEM images; (e) AFM image; (f) detail of the red square; (g) height profile of the 'hill' and 'sphere' along the red line in (e).

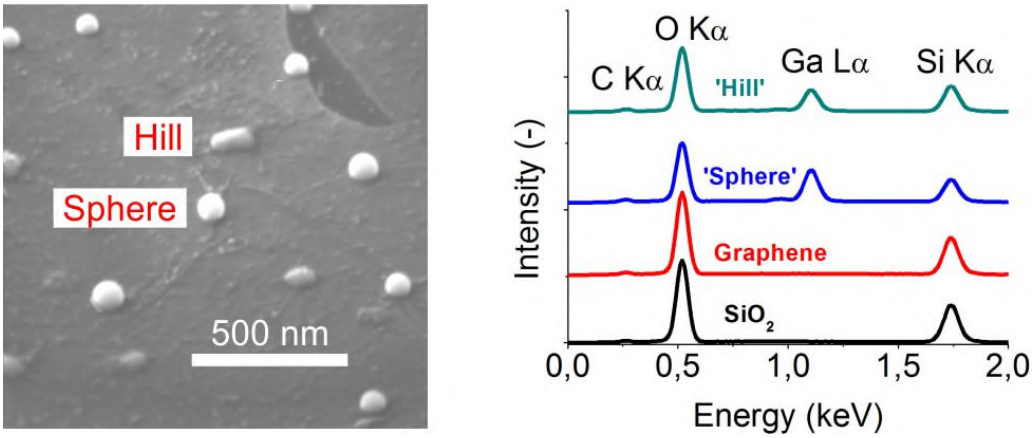

Figure 6.2: Left: Detailed SEM image of 'sphere' and 'hill' islands. A stage tilt is 58°. Notice much larger wetting angle for the spheres than for hills. Right: Both types of islands are composed of gallium as showed by EDS spectra.

Ga peak for the sphere is slightly more intense because the spherical island is higher and thus more Ga signal is detected. Origin and big height of the O peak and Si peak are pretty straightforward as the substrate is silicon dioxide. Tilted SEM image in the same figure shows the main difference between hill and sphere which is the wetting angle. Although, to say precise number would be uncertain we can tell the wetting angle for the spheres is much higher than 90° and for the hills it is around 90°.

6.1 Preview Raman measurement

Having more than micrometer distances between Ga islands, an idea come to us to measure the Raman map and hopefully detect Raman enhancement by individual gallium islands. Utilising TESCAN RISE device with microRaman laser spot of 1 µm diameter and the spatial resolution of 360 nm, we created Raman maps of the large-island sample. The map is 50 by 50 px^2 large and covers $5 \times 5\,\mu m^2$. Integration time for each spectrum in the map is 0.1 s and we use 7 mW of 532 nm laser. SEM scans of the measured area were taken before and after the measurement to be sure Ga islands were left intact. In Fig. 6.3 there are extracted information from the map. Fig. 6.3 (a) shows G peak area count of the 150 cm^{-1} width centered at 1595 cm^{-1}. The area covers SiO_2 in the top left corner and the rest is part of the graphene flake with Ga islands. Clearly, considering the extracted spectra in the (c), there are parts on the sample which enhance and also red-shift (b) all the D, G and 2D peaks of the Raman spectrum. By correlating the Raman map with SEM image aquired at the same place we were able to identify Raman spectrum for each Ga island. Correlated RISE image in Fig. 6.4 reveals an amplitude of the enhancement varies from island to island and on top of that, it seems that Ga spheres enhance the spectrum very little. After analyzing the map, there was an indication that Raman enhancement depends on the island size. To put speculations aside we measured bigger map with more Ga islands.

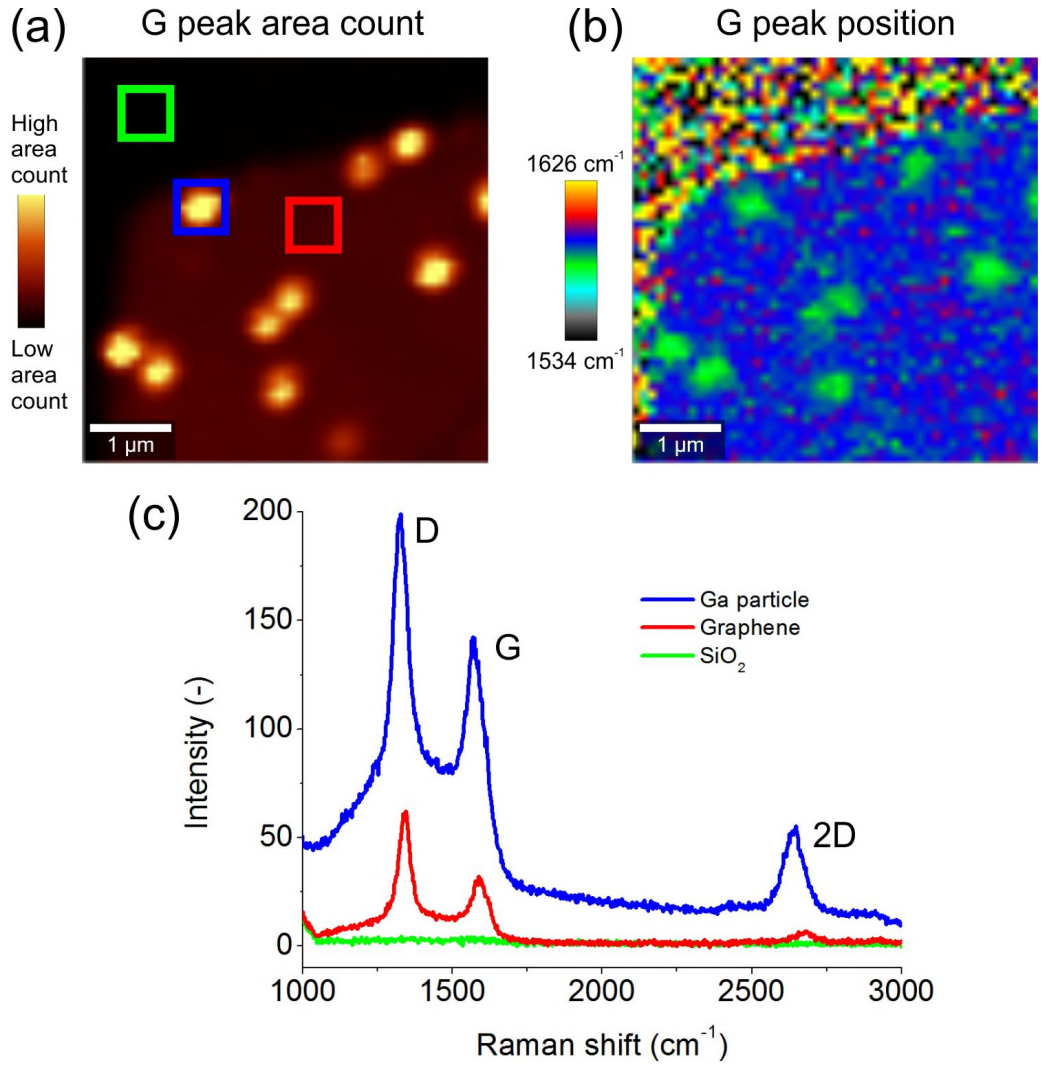

Figure 6.3: Raman map of the large-island sample. (a) G peak area count of width $150\,\mathrm{cm}^{-1}$ centered at $1595\,\mathrm{cm}^{-1}$. (b) G peak position. (c) Raman spectra extracted from the Raman map as represented with coloured squares in (a).

6.2 Raman enhancement

Follow-up Raman map covers $7.5 \times 7.5\,\mu\mathrm{m}^2$ of the sample area with the same pixel density than the preview map and more than fifty Ga islands in it. Integration time was 0.5 s per spectrum. Extracted G peak area count and D peak position are in Fig. 6.5. Raman signal is amplified over the islands. D peak, as seen in Figure and also G and 2D peaks are shifted to lower wavenumbers.

Characteristic Raman peaks of graphene were analysed with respect to individual Ga islands and are plotted in Fig. 6.6. Average of nine Raman spectra from 3 by 3 pixels area was assigned to each processed island. Peaks were fitted with Lorentzian functions that gave the values about intensity and position of the peaks. Height and position were plotted against 'equivalent sphere radius' defined as the radius of the sphere with the same projected area as the island. Island areas were determined in Gwyddion software using the SEM images. Even though, the projected shape of the islands is various from perfect circles (Ga spheres) to irregular islands, areas were determined with

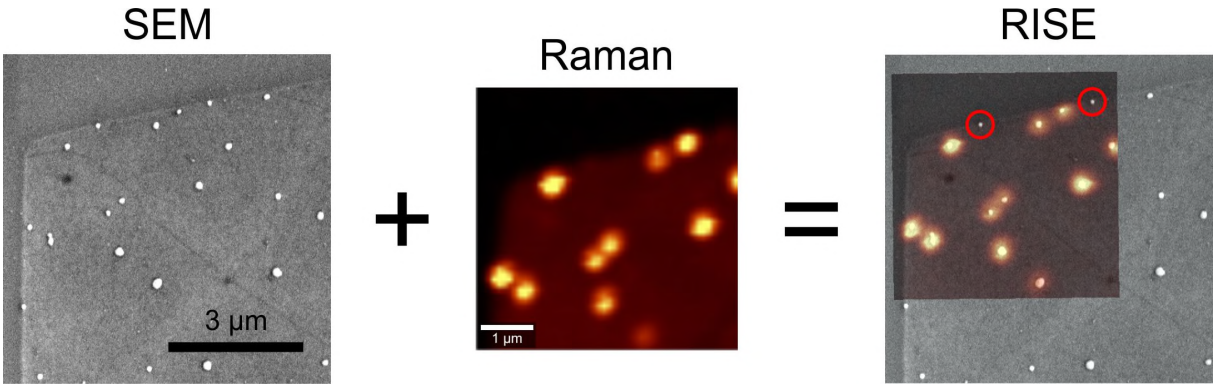

Figure 6.4: Raman imaging and scanning electron microscopy (RISE) technique allows us to correlate the SEM image with Raman map to identify which surface features are the source of strong Raman signal. Almost all the Ga islands are sources except two encircled ones and these are the only two 'spheres' covered by the Raman map. 'Hills' are much stronger sources.

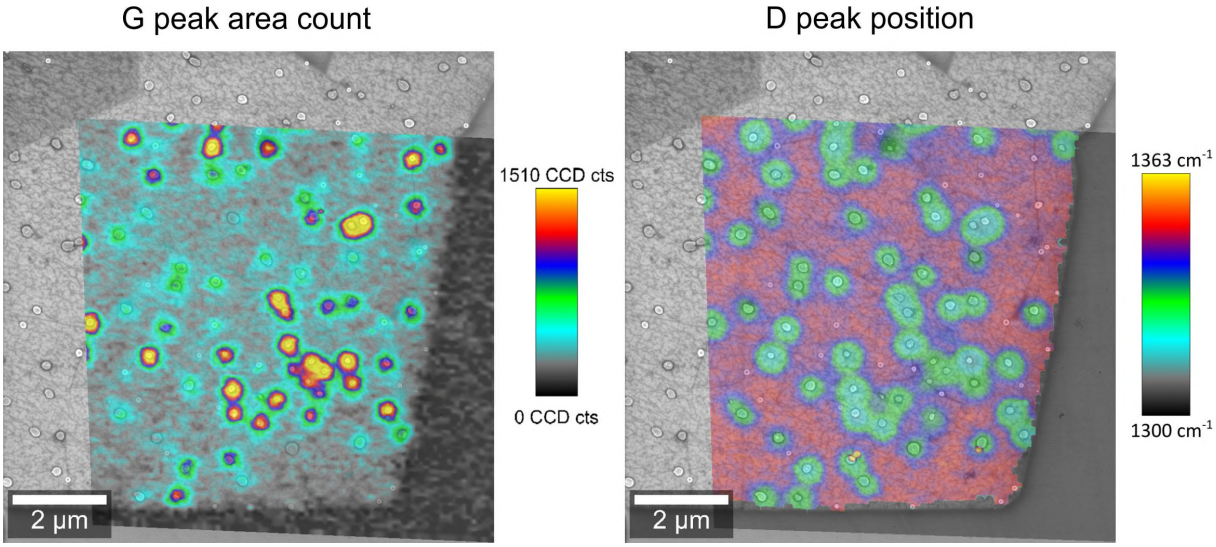

Figure 6.5: Detailed Raman map correlated with SEM images. Raman enhancement is presented with the G peak area count and the D peak position shows shifts. Size of the map is $75 \times 75\,\mathrm{px}^2$ with 0.5 s integration time per spectrum.

a high accuracy. By comparision of different Gwyddion methods for island selection together with manual adjustments resulted in the maximum area deviation of 3 %. Back to graphs, there is a clear dependence of the peak intensity and the peak position on the Ga island size. Not only the peaks but whole Raman spectrum is enhanced. The maximum enhancement is aproximately for 70 nm equivalent sphere radius. We attributed increased Raman intensity to Surface-enhanced Raman scattering (SERS) [26]. Incident electromagnetic wave, laser, is strongly electromagnetically enhanced due to plasmonic effects resulting from presence of Ga island. Amplified Raman scattered wave emanates from amplified incident wave. Out of the two mechanism, known to be behind the SERS, electromagnetic (plasmonic) enhancement contributes the most.

Interaction of Ga island and incident laser results in electron cloud displacement and thus, polarisation of Ga islands. This effect is known as Local surface plasmon polariton (LSPP) and causes an electromagnetic enhancement in the vicinity of island. Ga particle

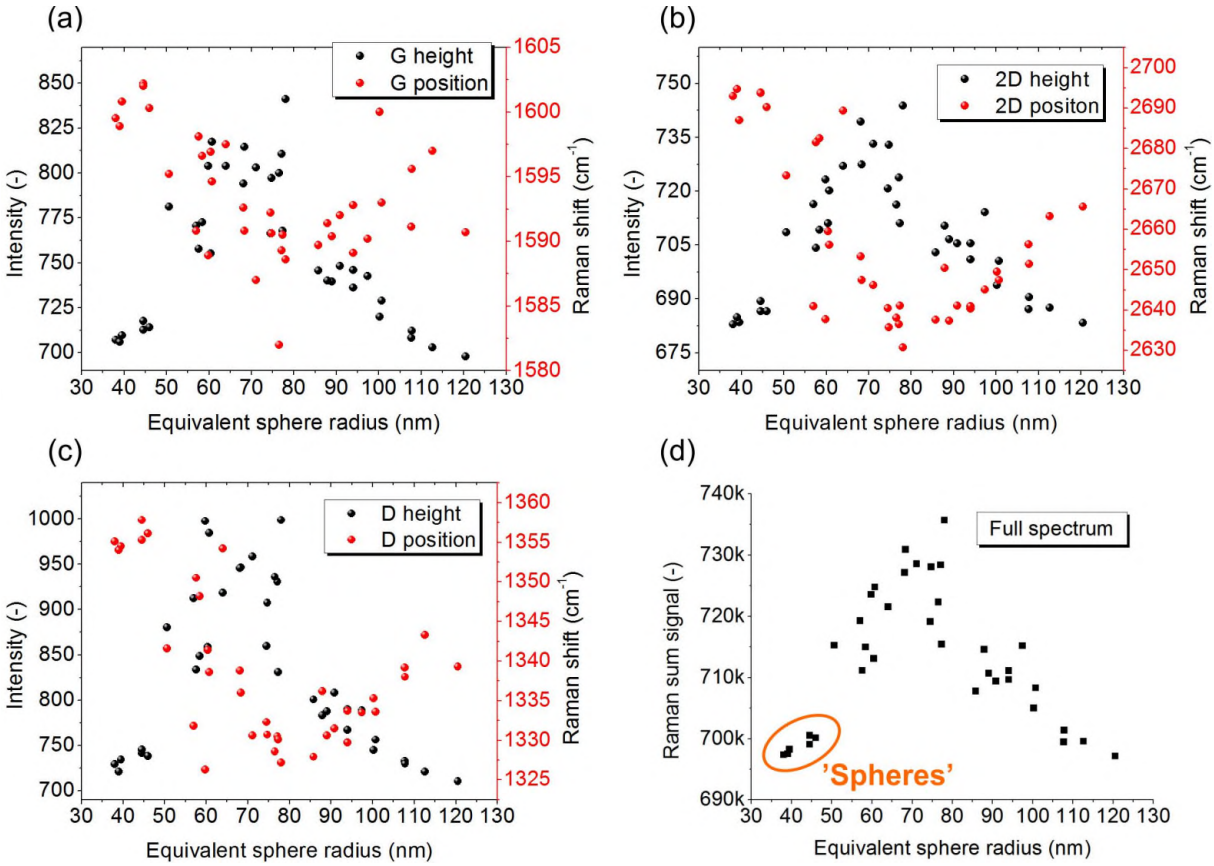

Figure 6.6: Raman peaks versus Ga island size. (a) G peak, (b) 2D peak a (c) D peak height and position with respect to the Ga equivalent sphere radius. (d) Sum of full Raman spectrum. Ga 'spheres' are marked with the ellipse. All other point were measured over 'hills'. Equivalent sphere radius is a radius of the sphere with the same projected area as the Ga island.

acts as a dipole antenna and emits light. Resonant position of LSPP also known as Local surface plasmon resonance (LSPR) depends on size and shape of the islands. We assume that the resonance for 532 nm laser arises at around 70 nm equivalent Ga sphere radius, the place with the strongest Raman signal.

To shed some light on our assumptions we simulated the experimental scenario. We aproximated Ga islands and spheres with the hemispherical Ga model. In Lumerical software, a plane wave was directed at SiO_2 substrate with Ga hemisphere on top as depicted in Fig. 6.7. Simulations were done for hemispheres from 30 to 120 nm of radii. A dielectric function of Ga was taken from the experimental work [23]. Our simulated near-field enhancement with respect to the incident wavelength is in Fig. 6.7. Enhancement is read from the detection spot as illustrated next to the graph. The detection spot is 10 nm to the right and 5 nm upwards from the point of contact between the Ga hemisphere and SiO_2. Calculated maximum field enhancement in the Raman shift range (grey rectangle in the graph) is maximum for the 80 nm sphere. It is in agreement with the measurement when we consider aproximation of the Ga particle. Maxima of the simulated field enhancement curves are LSPR with respect to the wavelength for each hemisphere. The electromagnetic mechanism could be definitely proved by using excitation laser of different wavelength. In that case the maximum enhancement would be for Ga island of different size according to the simulated results.

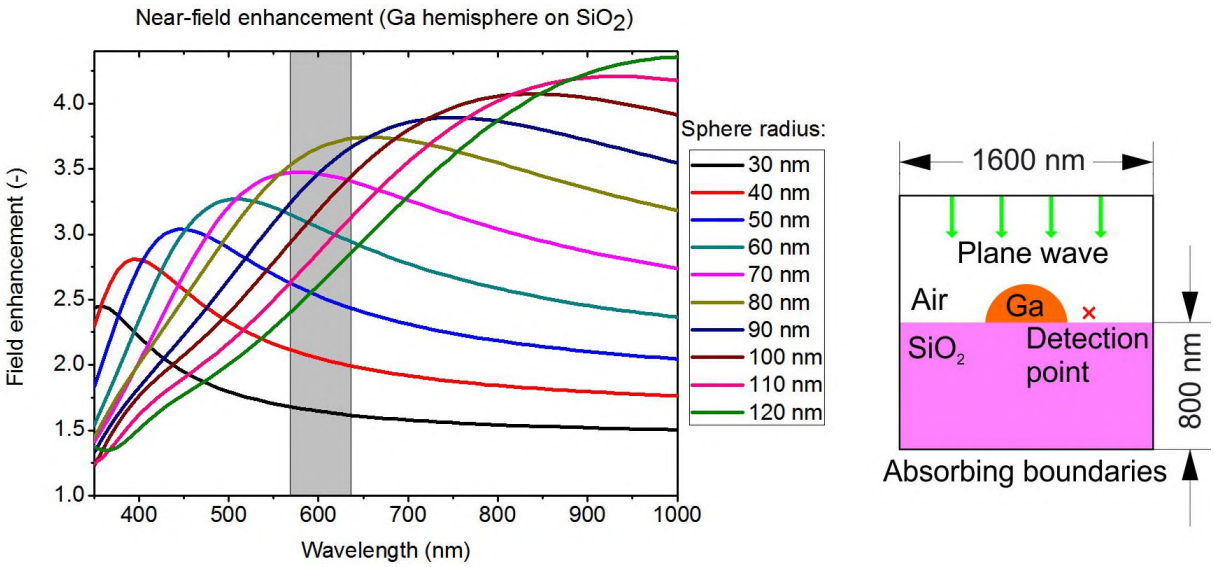

Figure 6.7: Simulation of the near-field enhancement of an incoming plane wave on the Ga hemisphere. Grey area in the graph is domain of Raman measurement with 532 nm excitation laser. Schematics of the simulation model is on the right. Detection point is 10 nm to the right and 5 nm upwards from the Ga/SiO_2 contact point. Simulated in Lumerical software.

From the previous simulation,enhancement for the single specific wavelength, 532 nm Raman excitation laser, was extracted. Simulated enhancement was put into graphs together with experimentally measured enhancments for D, G and 2D peaks. Graphs are in Fig. 6.8. Sphere radius is label for both datasets, 'equivalent sphere radius' of Ga islands and also 'hemisphere radius' from the simulation. From raw simulated data, enhancement of the 120 nm hemisphere radius was subtracted. Data were normalised with respect to the maximum enhancement value. Measured data were processed in a similar manner. Enhancement of the 120 nm sphere radius was substracted (this point was chosen, because it do not fluctuate as other data points, especially near the maximum). Then the data were normalised with respect to the average enhancement value for the spheres between 60 – 80 nm. Despite the facts that Ga does not form hemispheres and is covered with Ga_2O_3 layer, the agreement of the measured data with the simulation is obvious.

Another mechanism behind SERS is the chemical enhancement. Effects contributing to this mechanism are chemical interactions between the island and graphene and resonant excitation of charge-transfer state between the island and graphene [10][22]. However, Ga p orbital do not react with graphene π band, so the chemical interaction is minimal and our experimental results fits with the simulation and can be explained by plasmonic enhancement as the main contributor. Chemical enhancement could be hidden in the little deviations of measured data from the simulation.

6.3 Raman shift

Except the enhancement, Ga islands create another effect on the Raman spectra. All the graphene peaks are shifted. While the simulation explains observed enhancement, peak shifts are left to resolve. The second glance at Fig. 6.6 prompts to believe Raman shifts

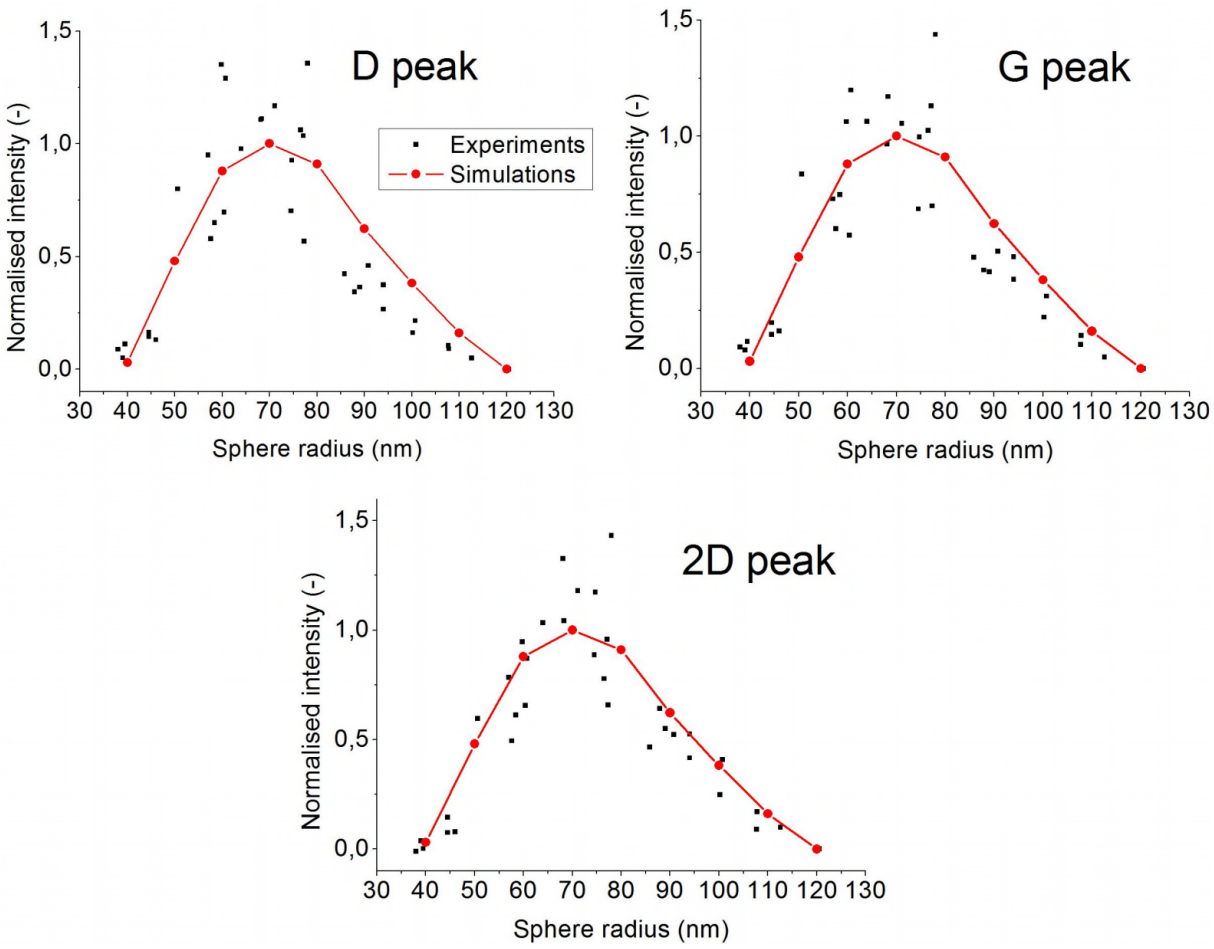

Figure 6.8: Raman enhancement of the peaks together with simulation. Red curve connecting the simulated data is a guide for the eye.

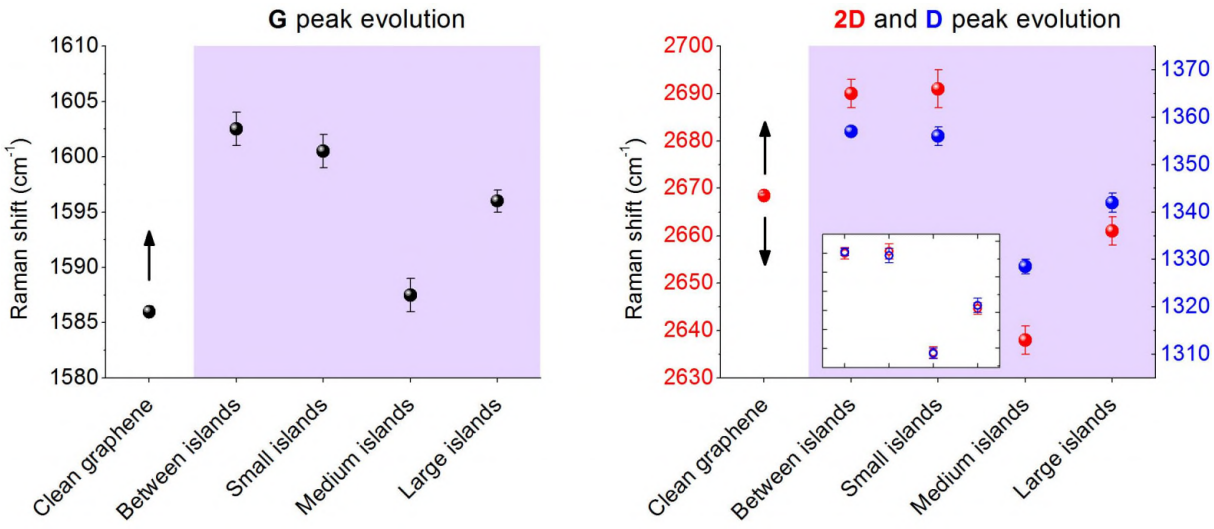

Figure 6.9: Raman peaks evolution from clean graphene through Ga deposited sample. Points for sample with Ga have light-blue background. Raman shift scales for the 2D and D peak have the same magnitude. Inset shows the mutual 2D and D peak position is the same after the y axis of the D peak position is rescaled.

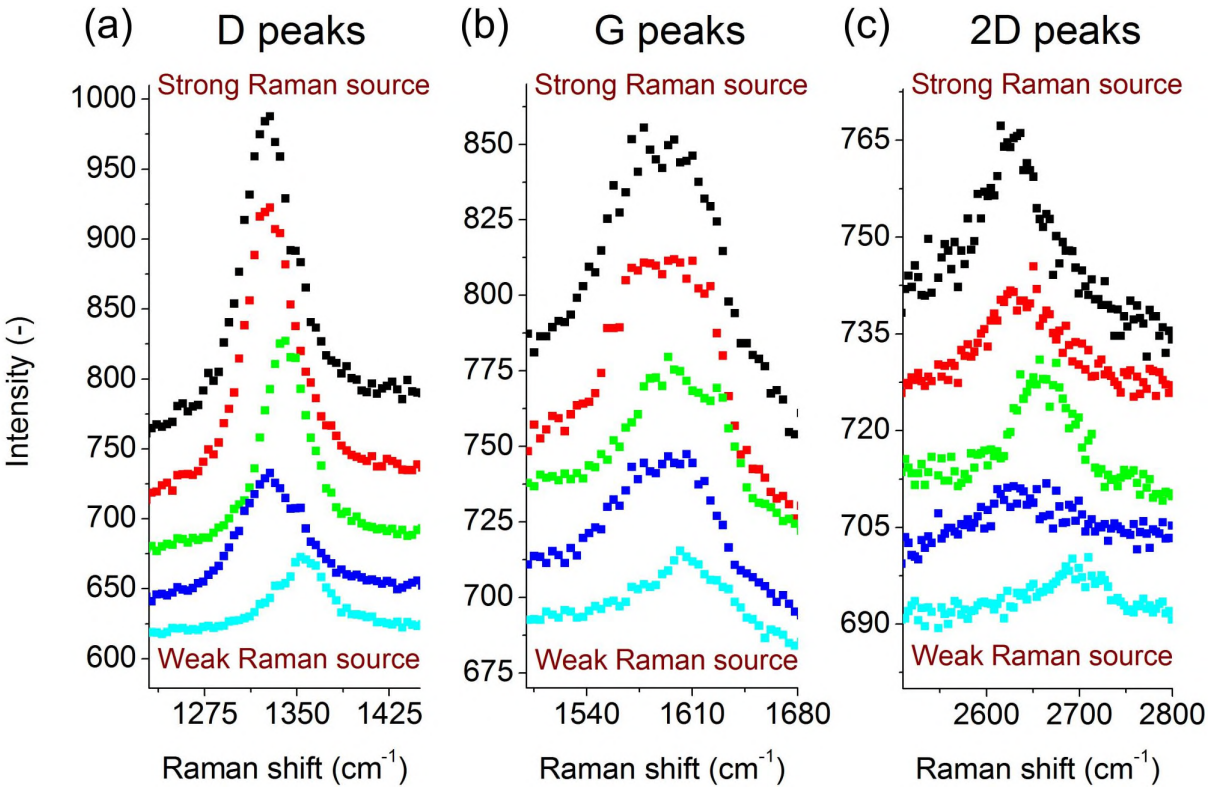

Figure 6.10: Detail on the characteristic graphene Raman peaks. Peaks are ordered from the lowest enhanced (Weak Raman source) to the highest enhanced (Strong Raman source). Legend to colours put as 'colour - equivalent spere radius (relative Raman sum signal)': sky-blue - 44.5 nm (0.04); blue - 77.1 nm (0.24); green - 60.4 nm (0.30); red - 76.5 nm (0.48); black - 74.1 nm (1).

are related to intensity. However, apparent indirect proportionality between Raman shift and Raman intensity cannot be explained by the means of plasmonic enhancement.

From the pristine graphene to the places on the sample with largest islands, characteristic graphene peaks evolve. G and 2D together with D peak shift evolutions are in Fig. 6.9. G peak shifts to higher wavenumber at the places in between the islands, where Ga threads of height about 6 nm are (60 min image in Fig. 5.5), then the peak slightly decreases at the small islands, decreases more rapidly at the medium-sized islands, where the Raman enhancement is the highest and finally with the large islands the G peak increases again. 2D peak evolution is similar except the peak is not shifted when measured in between the Ga island or at the small islands and the peak drop from small to medium-sized islands is much steeper. D peak shift is qualitatively similar to 2D peak shift. Approximate magnitude of the shifts is 52 cm^{-1} for the 2D, 29 cm^{-1} for the D and 17 cm^{-1} for the G peak. y-axes of the 2D and D peak evolution have the same scale. In the inset of the graph, the y-range for the D peak is rescaled to show the evolution of two peaks is the same. This could be related to the similar phonon mechanism behind the peaks origin, where 2D is overtone of D.

To sum it up, G peak is blue-shifted with Ga deposition and the D together with 2D peak can be both blue- or red-shifted depending on the Ga island size. Peaks in Raman spectrum of graphene can be shifted as the result of change in a carrier concentration due to doping or gating as shown in Fig. 3.5. Doping effect on the peak shifts is probably

not our case. For sure, graphene is n-doped by gallium, but it is doped homogenously and we measured variation of the peak position on the same sample. Next to that, we do not suppose there are any bound charges at the Ga/graphene interface, as Ga restores graphene lattice, or bound charges in a very thin gallium(III) oxide layer formed on the surface of Ga islands. Another reason against the peak shift caused by doping is that the peak shift evolution behaves differently for doped graphene and for our sample which is seen when comparing Fig. 3.5 (b), (c) with Fig. 6.9.

The shape progession of the Raman peaks as their intensity incease is in Fig. 6.10. D, G and 2D peaks tend to red-shift when enhanced. When graphene is under uniaxial strain the peaks also shift to lower wavelengths as shown in Fig. 3.6. Ga could stretch the graphene lattice and thus to cause peak shifts. D and 2D peak in Fig. 6.10 have Lorentzian shape, while G peak broadens with increasing intensity and is composed of two Lorentzian functions. We could say it splits just like the G peak of the uniaxially strained graphene splits into two components - G^+ and G^-. Nonetheless, Ga islands in our sample strain graphene multiaxially, so the G splitting could be influenced by tension in more than one direction. Strain is probably only one out of more mechanism for the peak shifting as it does not explain why the tension and so the Raman shift caused by Ga starts to reduce with large island size as seen in Fig.6.9.

Ga has showed to have at least two effects on graphene which could be studied by Raman spectroscopy. SERS is behind measured Raman enhancement and depends on the Ga island size. Simulation pointed out the enhancement is caused by the plasmonic mechanism. Apart from enhancement, Raman peaks are shifted due to strain of graphene lattice by adsorbed Ga islands.

7 Ga deposition on hydrogenated graphene

In this chapter, graphene treatment with atomic hydrogen is described and its effect on Ga deposition. Hydrogenation was perfomed with thermal cracker in the vacuum chamber with the base pressure 5×10^{-3} Pa. Thermal cracking is a dissociation of molecular hydrogen into atomic by contact with hot tungsten capillary. Hydrogen gas is let into the capillary which is heated by electron bombardement to 2000 °C. Electrons are accelerated from the tungsten filament by applying of 1800 V potential difference between the filament and the capillary. At these parameters, 100 % of hydrogen gas is dissociated. Sample was annealed to 150 °C before and hydrogenation took 2 h at RT. In order to compare the effect of hydrogenation on Ga deposition, we wanted to have a part of the graphene sample hydrogenated and another part clean. Little drop of A3 50PMMA (3% PMMA concentration in anisole with molecular weight 50000.) was placed on a part of graphene and the sample was heated at 100 °C for 10 min to remove excess anisole solvent. In optical microscope we noticed which flakes were covered with PMMA and which were not. PMMA should protect graphene from hydrogen adsorption. PMMA drop was removed in acetone. As it was not possible to use Ga effussion cell applied in previous experiments, the deposition on hydrogenated graphene sample was done with effusion cell from Createc in CEITEC. Prior to deposition, the sample was annealed at 150 °C for 1 h. The annealing temperature was chosen so that we are sure hydrogen would not desorb. The crucible of effusion cell was heated to 790 °C and the sample was kept at RT.

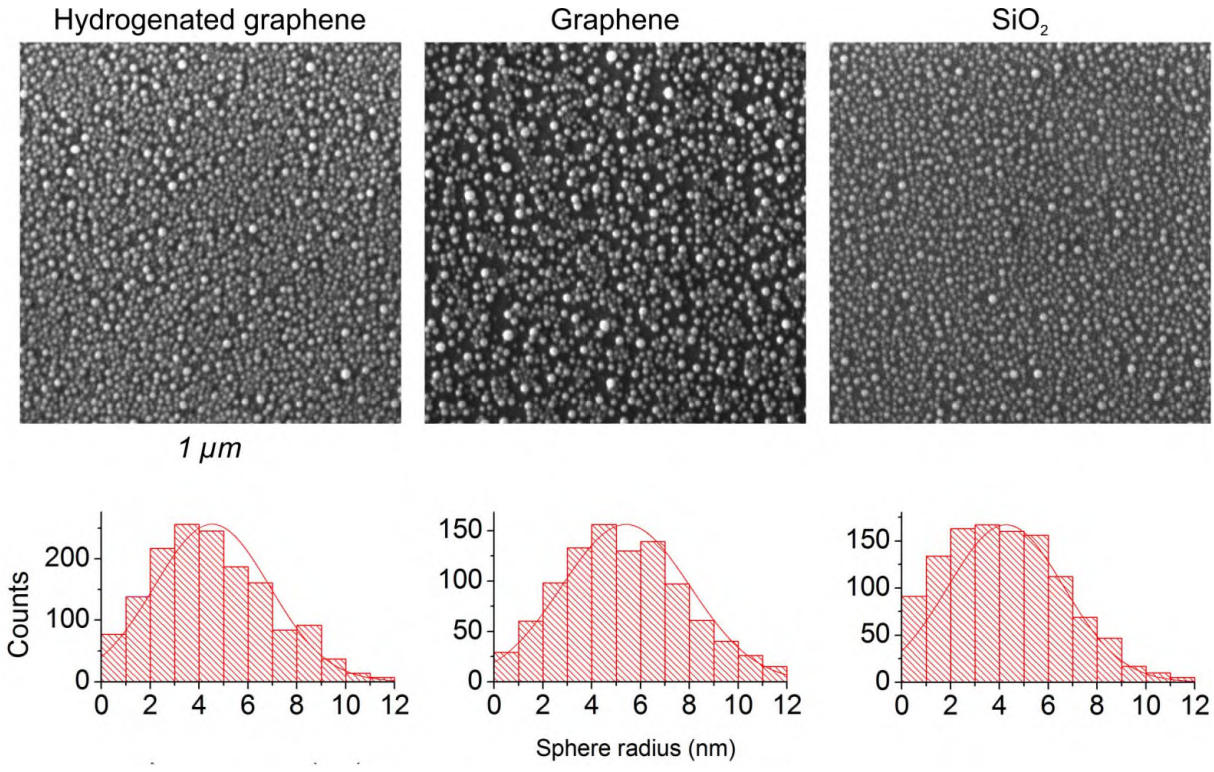

Figure 7.1: SEM images of hydrogenated and non-hydrogenated parts of the sample. Histograms are sphere sizes distributions from SEM images above.

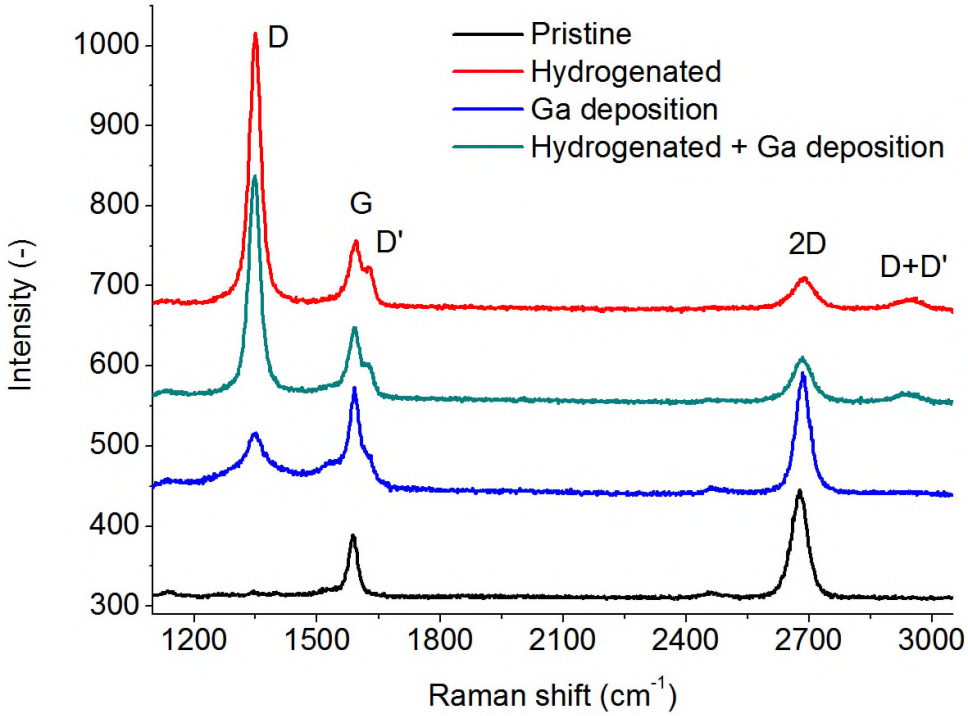

Figure 7.2: Raman spectra of Ga deposited on hydrogenated graphene. Spectra are offset for clarity.

SEM images of the sample after Ga deposition are in Fig. 7.1. Hydrogenation does make a difference in morphology of Ga deposited graphene monolayer. Average Ga sphere radius on graphene treated with atomic hydrogen is about a nanometer less than on pristine graphene. Also the Ga spheres are densely packed on hydrogenated graphene and together with smaller size they indicate the shorter diffusion length of Ga on hydrogenated graphene. Hydrogen adsorbed to graphene limits the diffusion of Ga. With SiO_2, there is no difference in the morphology of hydrogenated part and clean part. Hydrogen do not react with SiO_2. Sphere distributions on the sample are presented for each case below the images. Distributions are similar, we only point out decreased sphere size on hydrogenated graphene.

A glance at Raman spectra in Fig. 7.2 tells us Ga does not enhance hydrogenated graphene Raman spectra. Except that both hydrogenated graphene and Ga on hydrogenated graphene Raman spectra look almost the same indicating Ga does not influence phonon modes in graphene like in the case of Ga on clean graphene. Hydrogen plays a stronger role in Raman spectrum. As hydrogen atoms chemically attach to carbon atoms, they strongly disturb the electronic structure of graphene lattice resulting in emergence of D and D' peaks and diminishing the 2D peak.

8 Summary

In this diploma thesis we dealt with Molecular beam epitaxy (MBE) deposition of Ga on Chemical-vapour deposited (CVD) graphene. Aims of the thesis were also to study GaN on graphene and hydrogenated graphene as the substrate. Out of curiosity we prefered prefered to work with Ga on graphene into more details and to study interesting phenomena than to shallowly carry out all the tasks just for the sake of completing them.

In the theoretical part we described thin film growth by MBE with effusion cell as the source of depositing atoms. Next, graphene was presented together with its preparation techniques and analytic technique - Raman spectroscopy. Influence of strain, doping and temperature on the Raman spectra is shown. At last, properties of Ga/graphene and GaN/graphene are presented.

The experimental part deals with graphene, Ga/graphene preparation and analysis by Scanning electron microscopy, Atomic force microscopy, Energy-dispersive X-ray spectroscopy, X-ray photoelectron spectroscopy and Raman spectroscopy. We described preparation of CVD single-crystal graphene which is cleaner and better defined than the pollycrystaline version and characterised it. Graphene was transferred from a copper foil to SiO_2/Si substrates. Prepared graphene samples were further used for Ga depositions.

Depositions of Ga were arranged into two experiments. Both lead to the Volmer-Weber also known as island growth. In the first one, Ga was deposited at two different temperatures on Si(111) with native silicon dioxide layer on the top. We put emphasis on comparing the structure of Ga on graphene and SiO_2 in both experiments. Compared to SiO_2, increased diffusion length and thus larger Ga islands on graphene flakes were observed. The second experiment, with the sample at 300 °C, had a deposition duration as a variable. Ga formed two distinct structures - 'hills' and 'spheres'. Sphere radius had normal distribution. The radius of speheres increased with deposition time and was higher for graphene than for SiO_2. For the 2 h depositon, the distribution of Ga spheres on graphene was binormal.

Sample with large Ga particles showed Raman enhancement by individual Ga islands. Enhancement was island-size dependent and had maximum at medium-sized islands within the sample. The Raman enhancement was atributed to the Surface-enhancement which is utilised in Surface-enhanced Raman spectroscopy (SERS). A simulation was done to prove the Raman enhancement was caused by plasmonic enhancement of incident wave field by a Ga island. The plasmonic mechanism is stronger one of the two mechanism behind SERS. The other one is chemical mechanism, but as Ga does not react with graphene chemically, effect of this mechanism is minimal.

Next to Raman enhancement, Raman peaks were shifted and this was partially explained by the tensile strain of graphene lattice caused by Ga adsorbents. The explanation is based on G peak splitting into two components and the shift of both G and 2D peaks to lower wavenumbers. Furthemore, shift progression was the same for 2D and D peaks and different from the G peak behaviour. Since 2D is overtone of the D peak and they originate from the same transverse optical phonons, this is another indicator that strain is behind the Raman peak shifts. However, strain plays a role only for small and medium-sized islands, because from the Raman measurement, graphene becomes relaxed with large islands and the peak shift is reduced.

In the last part of the experimental section, we exposed the graphene sample to atomic hydrogen to fully hydrogenate it. We observed reduced Ga sphere size on hydrogenated

graphene indicating lowering the diffusion length of Ga atoms. The Raman spectra for hydrogenated graphene and for Ga on hydrogenated graphene are qualitatively the same. Chemical adsorption of hydrogen to graphene has the dominant effect on the Raman spectrum in contrast with weak interaction of Ga and graphene.

Effects of Ga on graphene such as strain of the lattice and doping can be studied using Raman specroscopy and deeper with polarised Raman spectroscopy which detects only specific Raman modes depending on the polarisation orientation. Also, Ga on graphene deposited with MBE could by utilised as the SERS substrate for detection of low-concentration elements, otherwise invisible in the Raman spectrum.

9 Bibliography

[1] Cgri. http://www.cgri.gr/k/QCL.html. Accessed: 2016-05-07.

[2] Cnx. http://cnx.org/contents/CyYU5KqY@2/Molecular-Beam-Epitaxy#id93333. Accessed: 2016-05-07.

[3] Gansystems. http://www.gansystems.com/why_gallium_nitride_new.php. Accessed: 2016-05-07.

[4] Omicron effusion cell. http://www.scientaomicron.com/cache/media_wez06_p1205%5B2034%5D_omicronmedia_image_paddedthumbnailscheme_ffffff_800x1200.jpg. Accessed: 2016-05-07.

[5] Balushi, Z. Y. A., Miyagi, T., Lin, Y.-C., Wang, K., Calderin, L., Bhimanapati, G., Redwing, J. M., and Robinson, J. A. The impact of graphene properties on GaN and AlN nucleation. *Surface Science vol. 634* (2015), 81–88.

[6] Berger, C., Song, Z., Li, T., Li, X., Ogbazghi, A. Y., Feng, R., Dai, Z., Marchenkov, A. N., Conrad, E. H., First, P. N., and de Heer, W. A. Ultrathin epitaxial graphite. *The Journal of Physical Chemistry B vol. 108*, issue 52 (2004), 912–916.

[7] Bonini, N., Lazzeri, M., Marzari, N., and Mauri, F. Phonon anharmonicities in graphite and graphene. *Physical Review Letters vol. 99*, issue 17 (2007).

[8] Butler, S. Z., Hollen, S. M., Cao, L., Cui, Y., Gupta, J. A., Gutiérrez, H. R., Heinz, T. F., Hong, S. S., Huang, J., Ismach, A. F., Johnston-Halperin, E., Kuno, M., Plashnitsa, V. V., Robinson, R. D., Ruoff, R. S., Salahuddin, S., Shan, J., Shi, L., Spencer, M. G., Terrones, M., Windl, W., and Goldberger, J. E. Progress, challenges, and opportunities in two-dimensional materials beyond graphene. *ACS Nano vol. 7*, issue 4 (2013), 2898–2926.

[9] Chua, C. K., and Pumera, M. Chemical reduction of graphene oxide. *Chem. Soc. Rev vol. 43*, issue 1 (2014), 291–312.

[10] Cialla, D., März, A., Böhme, R., Theil, F., Weber, K., Schmitt, M., and Popp, J. Surface-enhanced Raman spectroscopy (SERS). *Analytical and Bioanalytical Chemistry vol. 403*, issue 1 (2012), 27–54.

[11] Das, A., Pisana, S., Chakraborty, B., Piscanec, S., Saha, S. K., Waghmare, U. V., Novoselov, K. S., Krishnamurthy, H. R., Geim, A. K., Ferrari, A. C., and Sood, A. K. Monitoring dopants by Raman scattering in an electrochemically top-gated graphene transistor. *Nature Nanotechnology vol. 3*, issue 4 (2008), 210–215.

[12] Denis, P. A. Chemical reactivity and band-gap opening of graphene doped with Gallium, Germanium, Arsenic, and Selenium atoms. *ChemPhysChem vol. 15*, issue 18 (2014), 3994–4000.

[13] Duplock, E. J., Scheffler, M., and Lindan, P. J. D. Hallmark of perfect graphene. *Physical Review Letters vol. 92*, issue 22 (2004).

[14] Elias, D. C., Nair, R. R., Mohiuddin, T. M. G., Morozov, S. V., Blake, P., Halsall, M. P., Ferrari, A. C., Boukhvalov, D. W., Katsnelson, M. I., Geim, A. K., and Novoselov, K. S. Control of graphene's properties by reversible hydrogenation. *Science vol. 323*, issue 5914 (2009), 610–613.

[15] Ferrari, A. C. Raman spectroscopy of graphene and graphite. *Solid State Communications vol. 143*, 1-2 (2007), 47–57.

[16] Ferrari, A. C., and Basko, D. M. Raman spectroscopy as a versatile tool for studying the properties of graphene. *Nature Nanotechnology vol. 8*, issue 4 (2013), 235–246.

[17] Ferrari, A. C., Meyer, J. C., Scardaci, V., Casiraghi, C., Lazzeri, M., Mauri, F., Piscanec, S., Jiang, D., Novoselov, K. S., Roth, S., and Geim, A. K. Raman spectrum of graphene and graphene layers. *Physical Review Letters vol. 97*, issue 18 (2006).

[18] Giesbers, A. J. M., Uhlířová, K., Konečný, M., Peters, E. C., Burghard, M., Aarts, J., and Flipse, C. F. J. Interface-induced room-temperature ferromagnetism in hydrogenated epitaxial graphene. *Physical Review Letters vol. 111*, issue 16 (2013).

[19] Giovannetti, G., Khomyakov, P. A., Brocks, G., Kelly, P. J., van den Brink, J., and Pedersen, K. Substrate-induced band gap in graphene on hexagonal boron nitride: Ab initio density functional calculations. *Physical Review B vol. 76*, issue 7 (2007).

[20] Herman, M. A., and Sitter, H. *Molecular beam epitaxy.* Springer-Verlag, Berlin, 1989.

[21] Hertz, H. On the evaporation of liquids, especially mercury, in vacuo. *Annalen der Physik vol. 17* (1882), 177.

[22] Jensen, L., Aikens, C. M., and Schatz, G. C. Electronic structure methods for studying surface-enhanced Raman scattering. *Chemical Society Reviews vol. 37*, issue 5 (2008), 1061.

[23] Knight, M. W., Coenen, T., Yang, Y., Brenny, B. J. M., Losurdo, M., Brown, A. S., Everitt, H. O., and Polman, A. Gallium plasmonics. *ACS Nano vol. 9*, issue 2 (2015-02-24), 2049–2060.

[24] Langmuir, I. Chemical reactions at very low pressures. i. the clean-up of oxygen in a tungsten lamp. *Journal of the American Chemical Society vol. 35*, issue 2 (1913), 105–127.

[25] Losurdo, M., Yi, C., Suvorova, A., Rubanov, S., Kim, T.-H., Giangregorio, M. M., Jiao, W., Bergmair, I., Bruno, G., and Brown, A. S. Demonstrating the capability of the high-performance plasmonic Gallium–graphene couple. *ACS Nano vol. 8*, issue 3 (2014), 3031–3041.

[26] McNay, G., Eustace, D., Smith, W. E., Faulds, K., and Graham, D. Surface-enhanced raman scattering (sers) and surface-enhanced resonance raman scattering (serrs). *Applied Spectroscopy vol. 65*, issue 8 (2011-08-01), 825–837.

[27] Mohiuddin, T. M. G., Lombardo, A., Nair, R. R., Bonetti, A., Savini, G., Jalil, R., Bonini, N., Basko, D. M., Galiotis, C., Marzari, N., Novoselov, K. S., Geim, A. K., and Ferrari, A. C. Uniaxial strain in graphene by Raman spectroscopy: G peak splitting, Grüneisen parameters, and sample orientation. *Physical Review B vol. 79*, issue 20 (2009).

[28] Nair, R. R., Ren, W., Jalil, R., Riaz, I., Kravets, V. G., Britnell, L., Blake, P., Schedin, F., Mayorov, A. S., Yuan, S., Katsnelson, M. I., Cheng, H.-M., Strupinski, W., Bulusheva, L. G., Okotrub, A. V., Grigorieva, I. V., Grigorenko, A. N., Novoselov, K. S., and Geim, A. K. Fluorographene. *Small vol. 6*, issue 24 (2010-12-20), 2877–2884.

[29] Nečas, D., and Klapetek, P. Gwyddion. *Open Physics vol. 10*, issue 1 (2012).

[30] Neto, A. H. C., Guinea, F., Peres, N. M. R., Novoselov, K. S., Geim, A. K., and Pedersen, K. The electronic properties of graphene. *Reviews of Modern Physics vol. 81*, issue 1 (2009), 109–162.

[31] Novoselov, K. S. Electric field effect in atomically thin carbon films. *Science vol. 306*, issue 5696 (2004), 666–669.

[32] Oura, K. *Surface science*. Springer, Berlin, 2003.

[33] Pedersen, T. G., Flindt, C., Pedersen, J., Mortensen, N. A., Jauho, A.-P., and Pedersen, K. Graphene antidot lattices. *Physical Review Letters vol. 100*, issue 13 (2008).

[34] Procházka, P. Preparation of grafen by method CVD, 2012.

[35] Raman, C. V. A new radiation. *Indian Journal of Physics vol. 2* (1928), 387–398.

[36] Tuinstra, F. Raman spectrum of graphite. *The Journal of Chemical Physics vol. 53*, issue 3 (1970), 1126–.

[37] Voitsekhovskii, A., Nesmelov, S., Dzyadukh, S., Vasil'ev, V., Varavin, V., Dvoretsky, S., Mikhailov, N., and Yakushev, M. Admittance of metal–insulator–semiconductor structures based on graded-gap hgcdte grown by molecular-beam epitaxy on gaas substrates. *Infrared Physics vol. 71* (2015), 236–241.

[38] Wallace, P. R. The band theory of graphite. *Physical Review vol. 71*, issue 9 (1947), 622–634.

[39] Yi, C., Kim, T.-H., Jiao, W., Yang, Y., Lazarides, A., Hingerl, K., Bruno, G., Brown, A., and Losurdo, M. Evidence of plasmonic coupling in Gallium nanoparticles/graphene/SiC. *Small vol. 8*, issue 17 (2012), 2721–2730.

[40] Zhang, Y., Zhang, L., Zhou, C., Kelly, P. J., van den Brink, J., and Pedersen, K. Review of chemical vapor deposition of graphene and related applications. *Accounts of Chemical Research vol. 46*, issue 10 (2013), 2329–2339.

[41] Zhu, L., Zhao, X., Li, Y., Yu, X., Li, C., and Zhang, Q. High-quality production of graphene by liquid-phase exfoliation of expanded graphite. *Materials Chemistry and Physics vol. 137*, issue 3 (2013), 984–990.